Calhoun
Institutional Archive of the Naval Postgraduate School

Calhoun: The NPS Institutional Archive

DSpace Repository

Theses and Dissertations | 1. Thesis and Dissertation Collection, all items

1959

Measurement of some rare earth gamma rays using a two meter bent crystal spectrograph

Walter, Thomas Joseph.; Webber, James Hamilton.

Massachusetts Institute of Technology

http://hdl.handle.net/10945/14416

Downloaded from NPS Archive: Calhoun

http://www.nps.edu/library

Calhoun is the Naval Postgraduate School's public access digital repository for research materials and institutional publications created by the NPS community. Calhoun is named for Professor of Mathematics Guy K. Calhoun, NPS's first appointed -- and published -- scholarly author.

Dudley Knox Library / Naval Postgraduate School
411 Dyer Road / 1 University Circle
Monterey, California USA 93943

NPS ARCHIVE
1959
WALTER, T.

MEASUREMENT OF SOME RARE EARTH GAMMA RAYS USING A TWO METER BENT CRYSTAL SPECTROGRAPH

THOMAS JOSEPH WALTERS
JAMES HAMILTON WEBER

DUDLEY KNOX LIBRARY
NAVAL POSTGRADUATE SCHOOL
MONTEREY CA 93943-5101

Naval Postgraduate School

MEASUREMENT OF SOME RARE EARTH GAMMA RAYS USING A TWO METER BENT CRYSTAL SPECTROGRAPH

8854

by

Thomas Joseph Walters
B.S., U. S. Naval Academy
(1949)
Nav.E., Massachusetts Institute of Technology
(1956)

and

James Hamilton Webber
B.S., U. S. Naval Academy
(1949)
S.M., Massachusetts Institute of Technology
(1955)
Nav.E., Massachusetts Institute of Technology
(1955)

SUBMITTED IN PARTIAL FULFILLMENT OF THE
REQUIREMENTS FOR THE DEGREE OF
MASTER OF SCIENCE

at the

MASSACHUSETTS INSTITUTE OF TECHNOLOGY
July 1959

Signature of Authors . . . . . .

. . . . . .

Certified by . . . . . .
Thesis Supervisor

Accepted by . . . . . .
Chairman of Departmental Committee
on Graduate Students

NPS Archive
1959
Walter, T.

Thesis
W225

DUDLEY KNOX LIBRARY
NAVAL POSTGRADUATE SCHOOL
MONTEREY CA 93943-5101

ACKNOWLEDGEMENTS

In concluding this thesis, it is a pleasure to express out gratitude to those people who have materially aided the furtherance of the project.

Professors Norman C. Rasmussen and Hans Mark both gave their time freely. Their advice and guidance were of constant assistance.

We are especially indebted to Dr. John Garfield of Brookhaven National Laboratory for the processing of the nuclear emulsions. Members of the M.I.T. Reactor Staff were of assistance in the source irradiation and in the development of the source handling equipment and procedures.

MEASUREMENT OF SOME RARE EARTH GAMMA RAYS USING A TWO METER BENT CRYSTAL SPECTROGRAPH

by

Thomas Joseph Walters

and

James Hamilton Webber

Submitted to the Department of Nuclear Engineering on July 27, 1959 in partial fulfillment of the requirements for the degree of Master of Science in Nuclear Engineering.

ABSTRACT

The assembly, alignment and initial operation of a two meter bent crystal spectrograph of the Cauchois type is described. Treatment is given to the auxiliary equipment necessary for handling and exposing radioactive sources of several curies strength. The research reactor at the Massachusetts Institute of Technology has been used to produce radioactive sources of several of the even Z rare earth elements between Z = 60 and Z = 70. These elements decay by beta emission or electron capture to excited states in odd Z isotopes. By exposing these sources in the spectrograph, photographic spectra were obtained of the more intense gamma rays emitted. The plates were calibrated with x-rays and gamma rays of known wavelengths. Energies of 17 gamma rays from 64 kev to 400 kev were determined with a precision of about one part in 2000.

Thesis Supervisor: N. C. Rasmussen

Title: Assistant Professor of Nuclear Engineering

TABLE OF CONTENTS

Letter of Transmittal

Acknowledgements

Abstract

Table of Contents

Section I - Introduction 1

Section II - Theory of the Bent Crystal Spectrograph

A. Bragg's Law 3

B. Geometric Optics of the Curved Crystal Focusing Spectrograph 5

C. Exact and Approximate Geometries 7

D. Source-Detector Arrangement 12

E. Instrument Efficiency Considerations 15

Section III - Description of Experimental Apparatus

A. Two Meter Bent Crystal Spectrograph 20

B. Quartz Crystal and Crystal Holder 23

C. Source Handling and Storage Equipment 25

D. Source Materials and Containers 32

E. Source Irradiation Facility 37

Section IV - Experimental Apparatus

A. Optical Alignment of the Spectrograph 39

B. Hartmann Tests 46

C. Source Positioning and Shielding 55

D. Source Irradiation and Handling Procedures 62

E. Detection Procedures 68

Section V - Data Reduction and Calculational Methods

A. Measurement of Line Positions 71

TABLE OF CONTENTS

Letter of Transmittal

Acknowledgements

Abstract

Table of Contents

Section I - Introduction 1

Section II - Theory of the Bent Crystal Spectrograph

A. Bragg's Law 3

B. Geometric Optics of the Curved Crystal Focusing Spectrograph 5

C. Exact and Approximate Geometries 7

D. Source-Detector Arrangement 12

E. Instrument Efficiency Considerations 15

Section III - Description of Experimental Apparatus

A. Two Meter Bent Crystal Spectrograph 20

B. Quartz Crystal and Crystal Holder 23

C. Source Handling and Storage Equipment 25

D. Source Materials and Containers 32

E. Source Irradiation Facility 37

Section IV - Experimental Apparatus

A. Optical Alignment of the Spectrograph 39

B. Hartmann Tests 46

C. Source Positioning and Shielding 55

D. Source Irradiation and Handling Procedures 62

E. Detection Procedures 68

Section V - Data Reduction and Calculational Methods

A. Measurement of Line Positions 71

B. Calculation of Gamma Ray Energies 73

C. Determination of Standard Deviation 77

Section VI - Results 82

Section VII - Conclusions and Recommendations

A. Conclusions 86

B. Recommendations 86

Section VIII - Appendix

A. Sample Calculations 88

B. Wavelengths of Calibration Lines 95

C. Bibliography 96

SECTION I - INTRODUCTION

The recent theory of nuclear structure developed by Bohr and Mottleson (1 , 2) makes predictions of the low lying energy levels of the nucleus. In heavy elements (beginning around Z = 60) the first few energy levels belong to the rotational band of the ground state. Previous measurements of rotational spectra have revealed small deviations from the rotational level sequence predicted by first order theory. The presence of certain higher order terms in the equations of the collective model appears to explain these deviations. It is highly desirable that energy levels of additional isotopes be measured so that the adequacy of the higher order terms of the theory can be verified. The deviation of these terms from first order theory is so small that this verification requires gamma ray energy measurements of high precision.

It is the purpose of this thesis to partially satisfy this need by application of a bent crystal diffraction technique by which gamma ray energies may be measured with a precision of up to one part in 3000. The precision decreases with increasing energy.

Measurements of this type have been previously made, starting in 1947, by DuMond (15) at California Institute of Technology with a focusing curved crystal gamma ray spectrometer. More recently, a group at the Radiation Laboratory, University of California, Livermore, California, (7 , 8 , 9) have used a slightly different geometry in conjunction with the A-48 accelerator to measure the gamma rays emitted in electric excitation processes.

This thesis describes the assembly, calibration and initial operation of a two meter focusing spectrograph of the Cauchois type. The experimental work was devoted to the measurement of gamma ray energies only, no attempt being made to determine the relative intensities of the radiations. Since the efficiency of the bent crystal spectrograph is a strong function of gamma ray energy, considerably more calibration work will be required before absolute intensity measurements are feasible.

Gamma ray energies of five odd Z rare earth elements, from Z = 61 to Z = 71 were measured. These gamma rays were emitted following beta decay or electron capture of radioactive even Z isotopes. Radioactive sources of several curies strength were produced in the research reactor at the Massachusetts Institute of Technology (24).

SECTION II - THEORY OF THE BENT CRYSTAL SPECTROGRAPH

A. BRAGG'S LAW

The operation of any crystal spectrometer or spectrograph is dependent on the diffraction of electromagnetic waves by the regularly spaced atoms in a crystal. Historically, the discovery of the resolving property of crystals grew from a suggestion by Laue. He suggested that a crystal, with its regular, three-dimensional array of atoms, might behave toward a beam of x-rays in somewhat the same way as does a ruled diffraction grating toward a beam of ordinary light. Subsequent experimental work(17) verified this postulate.

A simple and convenient way of looking at the process of diffraction by a crystal grating was proposed by Bragg (3) Reference(22)contains a lucid explanation of Bragg's Law for x-ray diffraction and may be consulted for a fuller treatment than that which follows.

If plane monochromatic electromagnetic waves are incident on the atoms in a crystal, a wavelet of scattered radiation will spread out from each atom in all directions.

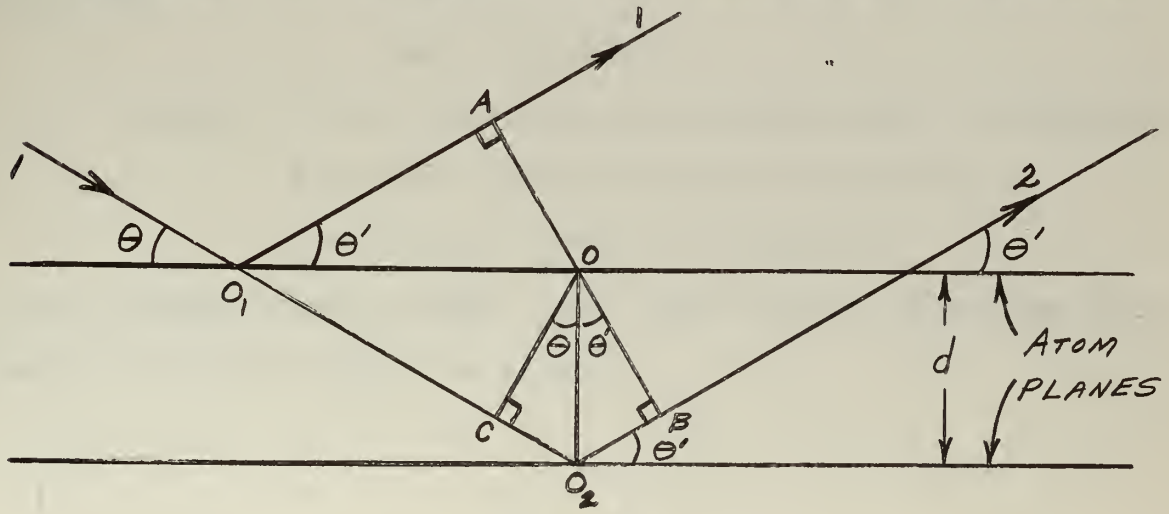

Figure 1

In Figure 1, the two horizontal lines represent two successive atomic planes in a crystal, where d is the crystal spacing for these particular planes, θ is the angle of incidence of the electromagnetic radiation on the planes and θ^1 the angle of reflection. The wavelets reflected from each of these parallel planes will combine, in general, in different phases and so will destroy each other by interference. However, there are certain conditions as to wavelength and angle of incidence where the waves from different planes will combine in the same phase and reinforce each other. These necessary conditions comprise Bragg's Law.

Constructive interference will occur if path $1O_1A$, taken by waves scattered at O_1, differs by an integral number of wave lengths from path $1O_2B$, taken by waves scattered at O_2. Assuming $\theta = \theta^1$, right triangles OAO_1 and OCO_1 are congruent, so $O_1A = O_1C$. Therefore, the condition for constructive interference becomes $O_2C + O_2B = n\lambda$. Since $O_2C = d \sin \theta$ and $O_2B = d \sin \theta^1$, this may be written $2d \sin\theta = n\lambda$.

The full condition that there be a reflected beam is therefore,

$$\theta = \theta^1$$

$$n\lambda = 2d \sin \theta$$

where: n is an integer, called the order of reflection

d is the spacing between atom planes

λ is the wavelength of radiation

In the present spectrograph, only first order reflections are used, so n may be taken as unity.

B. GEOMETRIC OPTICS OF THE CURVED CRYSTAL FOCUSING SPECTROGRAPH

Following the discoveries of Laue and Bragg in 1912, eighteen years passed before a practical scheme for a curved crystal, focusing spectrometer was published by DuMond and Kirkpatrick.(15) This paper, which states the principles of exact focusing with curved crystals was closely followed by papers (4,5,19, 20) describing the different approximate and exact realizations of these principles. The current literature contains several good descriptions of the curved crystal focusing spectrometer, references (11), (12), and (13) being examples.

The curved crystal spectrometer may be classified into two general types: the reflection case and the transmission case. The first curved crystal spectrometer of the reflection type was built by H. H. Johann (19) and the first transmission type, which is of the type used in this thesis, was built by Y. Cauchois (4) Figure 2, taken from reference (11), illustrates the exact transmission case.

A crystal is shown whose reflecting boundary coincides with part of the circle of center O. The short atomic reflecting planes traversing the thin crystal sheet all point to a common junction at C_1 called the beta point. In this type there is one real focus I and one virtual focus S.

To illustrate the focusing properties of this instrument, imagine an extended radioactive source at position A in Figure 2. Electromagnetic radiation emanating from this source in the form of x-rays or gamma rays of wave length λ_i strikes

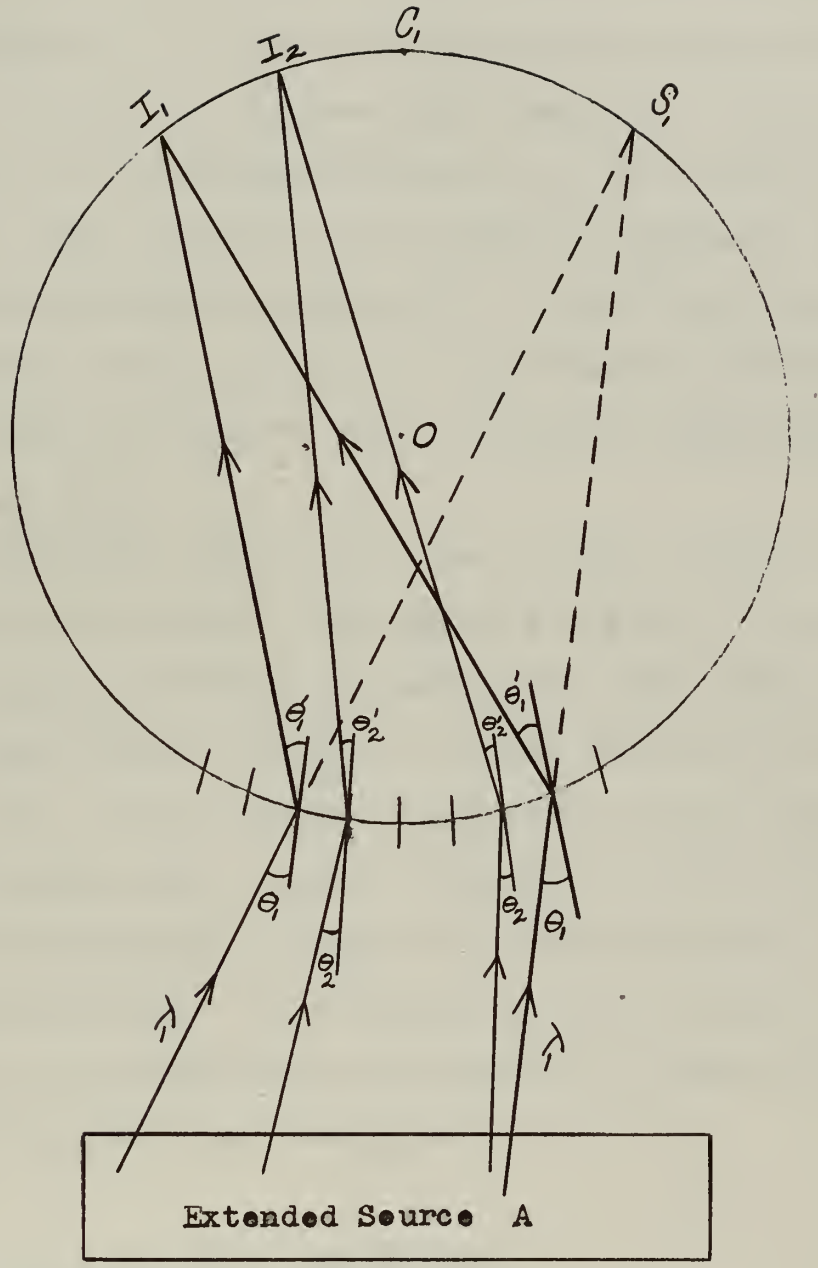

Exact Transmission Spectrograph

Figure 2

one of the atomic reflecting planes in the crystal at angle θi. If λ_1 and θ_1 satisfy the Bragg condition, $\lambda_1 = 2d \sin \theta_1$, reflection will take place, the reflected wave leaving the atomic plane at angle θ_1'. Now, picture another quanta of electromagnetic radiation of the same wave length λ_1, coming from another part of the extended source. If this quanta strikes one of the atomic planes of the crystal at angle θ_1 it will similarly be reflected at angle θ_1'. Since both atomic planes point toward point C_1, it can be seen that the reflected rays will be focused at point I_1, both angles θ_1 being subtended by the same arc I_1C_1.

Radiation from the source of wave length λ_2 will be reflected by the crystal, leaving at angle θ_2, in accordance with the Bragg condition. Focusing will again take place, but since θ_2 will differ from θ_1, the focal point will be at a new location, I_2. It is from the measurement of the distance I_1I_2, that the relative wave length differences of two x or gamma rays may be accurately determined. These are easily converted to energy differences. The present method of energy determination reduces to a straightforward measurement of distance from reference lines of known energies.

C. EXACT AND APPROXIMATE GEOMETRIES

The exact type of reflecting spectrometer has been constructed by suitably profiling the crystal lamina (in its unstressed state) to the required radius of curvature, twice the radius of the focal circle, and then bending it so that

the boundaries conform to the focal circle. In this case, the atomic reflecting planes in the bent crystal will then have a radius of curvature of just twice that of the focal circle.(20) Y. Cauchois realized that the position of the boundary of the crystal was considerably less important than the direction of the atomic planes. The Cauchois approximate type of transmission spectrograph makes use of this observation to avoid the difficult profiling of the boundary surface.

The Cauchois approximate type of spectrograph, of which the MIT two meter instrument is an example, requires no profiling of the crystal. An unstressed quartz crystal, whose (310) planes are perpendicular to its optically flat surfaces, is bent to a radius equal to the diameter of the focal circle. Thus, the reflecting planes all point to the beta point, but the crystal itself does not conform to the focal circle.

The chief geometrical aberration in the Cauchois approximate transmission type spectrograph comes from the fact that the neutral axis of the curved lamina deviates at its extremities from exact coincidence with the focal circle. Figure 3 shows the geometry of the relative line broadening, which results from this aberration. Reference gives the result

$$\frac{\Delta\lambda}{\lambda} \cong \frac{\cos\theta\,(1 - \cos\alpha)}{\cos(\alpha + \theta)}$$

where θ is the Bragg angle

α is the half-angle subtended by the crystal.

Clearly for small Bragg angles and small α, $\frac{\Delta\lambda}{\lambda}$ rapidly becomes negligible.

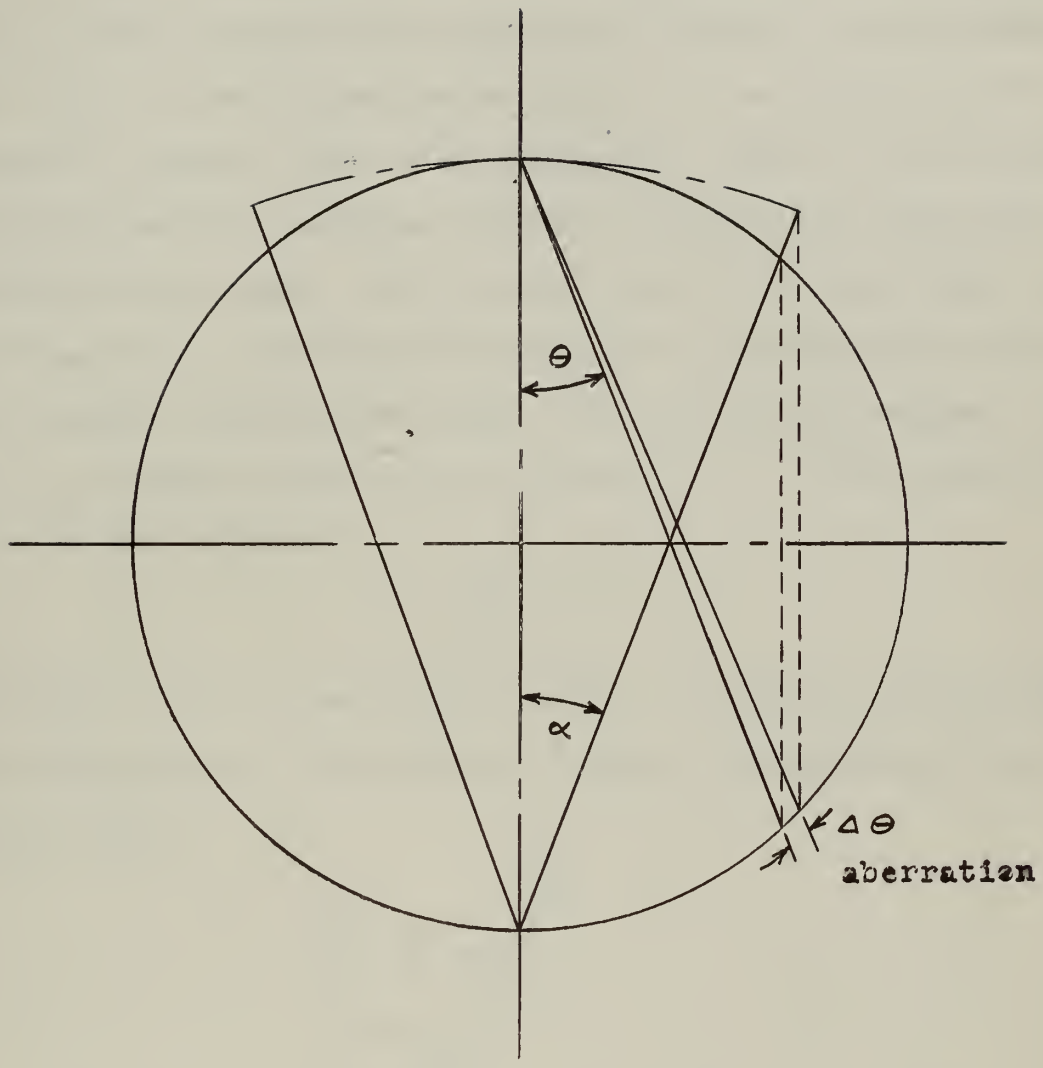

Cauchois Approximate Transmission Spectrograph

Figure 3

In the MIT two meter spectrograph, this fractional aberration is of the order of 10^{-5}.

An interesting result of the type of reflection taking place in the transmission type curved crystal spectrograph is that there is no correction whatever to the Bragg angle for the refractive index of the electromagnetic rays in the crystal, provided that the internal planes of reflection are normal to the crystal slab. This is not true of the reflection type spectrograph. Referring to Figure 4 we see that the ratio of the wave lengths outside and inside the crystalline medium, λ_1 and λ_2, respectively, will be equal to μ, the refractive index of the crystal:

$$\frac{\lambda_1}{\lambda_2} = \mu$$

The ratio of the sines of the angles, θ_1 and θ_2, of incidence and refraction at both entrance and exit boundaries of the crystal will

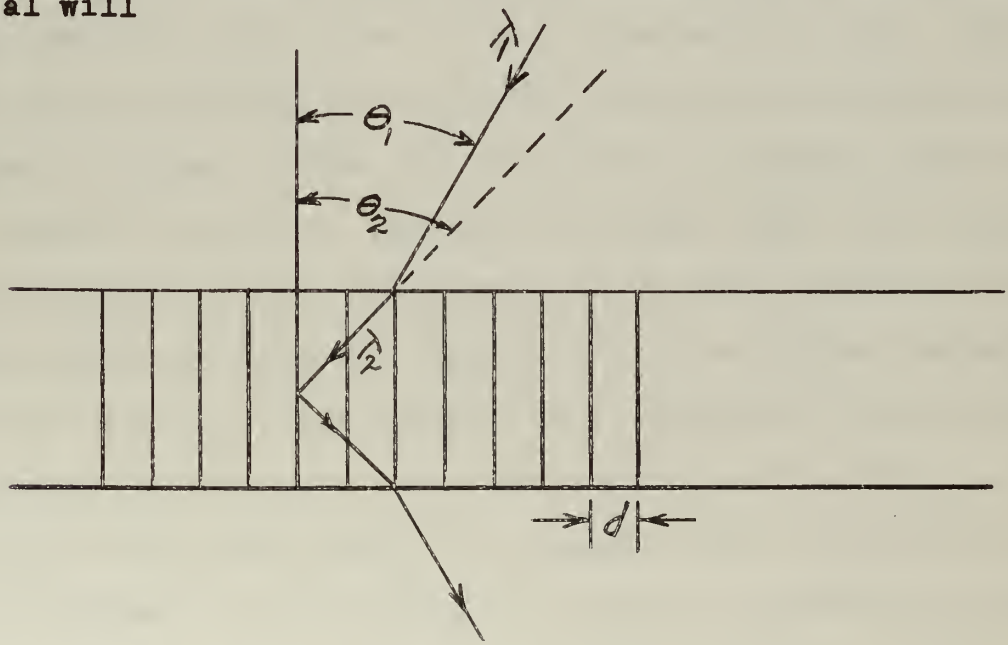

Refraction of Rays in Crystal

Figure 4

also be equal to

$$\frac{\sin \theta_1}{\sin \theta_2} = \mu$$

If the reflecting planes are normal to the boundary surface, the Bragg equation inside the crystal is

$$n\lambda_2 = 2d \sin \theta_2$$

Substitution from the previous relations quickly leads to the conclusion that

$$n\lambda_1 = 2d \sin \theta_1$$

This relation shows that the angle of reflection is independent of the refractive index of the crystal.

It has also been shown by Cauchois that, in the transmission case, there is a focusing effect through the thickness of the curved crystal sheet as well as from side to side. When the crystal lamina is curved, the strain near the outside (convex) surface of the plate results in a larger grating spacing than the strain free value at the neutral axis. The larger grating spacing results in a smaller Bragg angle at the outside. The opposite effect occurs for reflection by regions near the inner (concave) surface. DuMond (11) states that this results in exactly the required convergence of all the reflected beams over the entire thickness of the slab to give perfect focusing from front to back. This leads to the conclusion that in the transmission spectrograph it is the neutral axis of the crystalline slab which must be in contact with the focal circle. This observation is used during the optical alignment to choose a point on the crystal as a reference for the focal circle.

D. SOURCE - DETECTOR ARRANGEMENT

Two possible geometries for use with the transmission type, curved crystal spectrometer are shown in Figure 5.

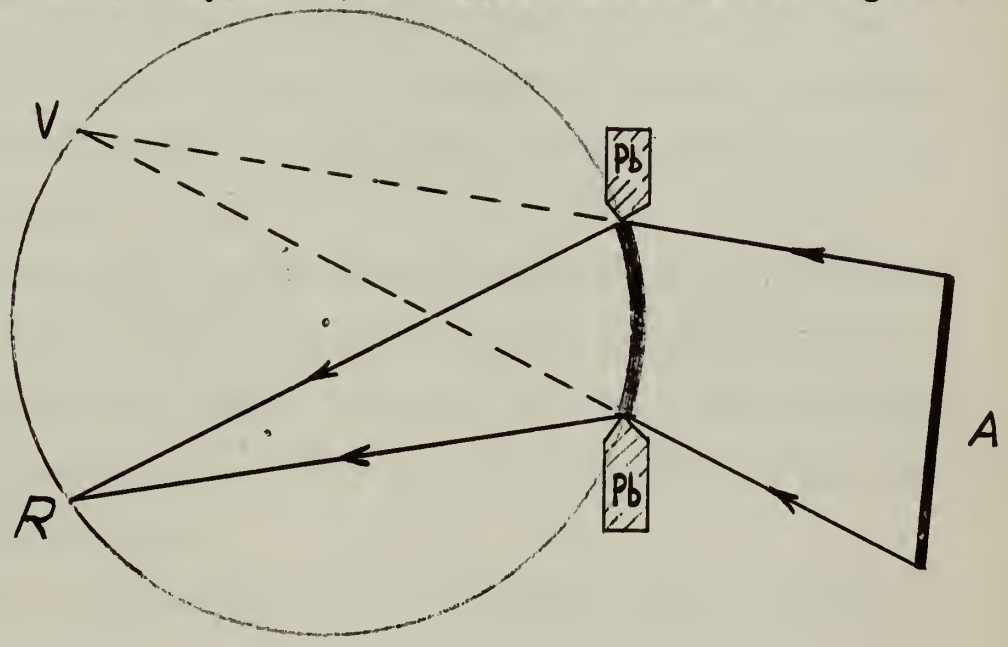

Scheme I

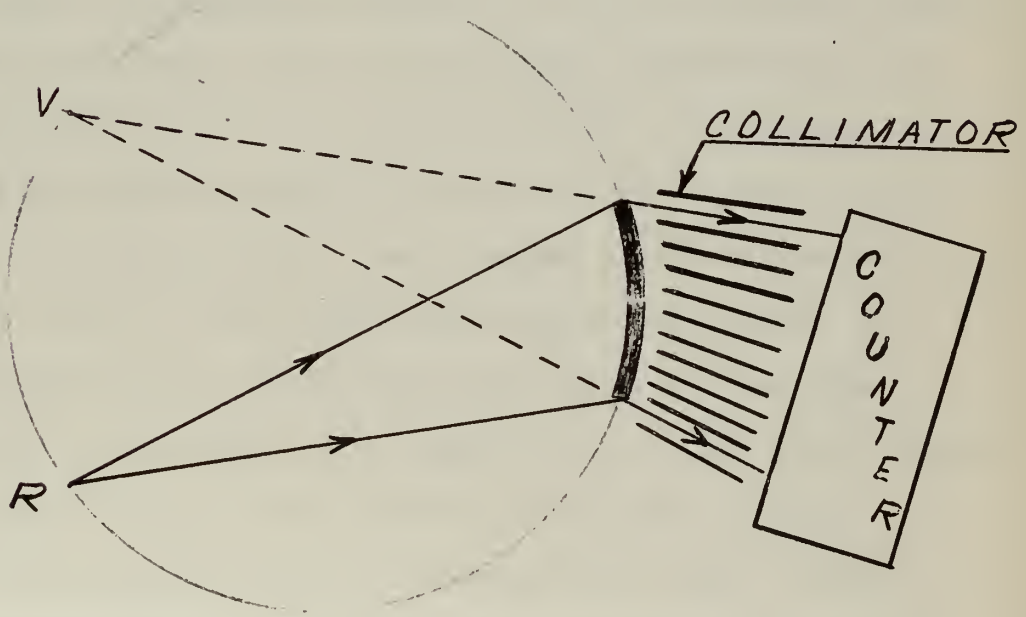

Scheme II

Figure 5

In scheme I, we place an extended source at A, measuring the various x and gamma ray energies by the displacement of the focused lines, along the focal circle. Detection in this case is feasible by either a photographic emulsion placed along the focal circle or a counter behind a suitable slit arrangement. Such a photographic spectrograph was first used by Cauchois.

DuMond (11) has extensively developed the alternate scheme, wherein a very concentrated source is placed at the focus, R, and the intensity, measured in a GM or scintillation counter, is plotted as a function of the position of the source R on the focal circle.

For a source of a given strength, use of scheme II permits the attainment of somewhat higher monochromatic intensities. This may be seen from the following considerations. For a very thin concentrated source at R, every atom can radiate the specified wavelength into a solid angle subtended by the entire working aperture of the curved crystal. In scheme I, however, for an emitted gamma ray line of a given wave length, each nucleus at some point in the extended source placed at A, can only make use of a very small solid angle subtended by a very thin portion of the curved crystal where the incident radiation strikes the reflecting planes at just the right Bragg angle. A study with the two crystal spectrometer using unstressed flat quartz plates has established that, for the (310) planes of quartz, the selective reflection of a given wave length is restricted to an angular region of the order of

only a few seconds of arc(25). This is to be compared to a horizontal angular opening of approximately 1.5 degrees in scheme II.

The above arguments in favor of scheme II, as advanced by DuMond(11), are largely neutralized when consideration is given to the geometrical configuration of the radioactive source. In scheme II adequate resolution of gamma ray energies requires that quite thin sources be used. DuMond (13) has used rectangular strips of metal, such as tantalum or gold of dimensions 30mm X 5mm X .05mm, the thin dimension being that vertically along the focal circle. In the arrangement of the MIT spectrograph (scheme I), however, source sizes of one inch diameter cylinders are easily used. Therefore, advantage may be taken of the extended source position in the scheme I geometry to use considerably stronger sources, gaining back much of the intensity lost to the smaller angular acceptance angles around the correct Bragg angle.

The prime advantage of the scheme I geometry is its absence of moving parts. Figure (7) is a photograph of the MIT two meter spectrograph. The simplicity of the arrangement is apparent. The lines are all formed simultaneously over a considerable segment of the spectrum in a single exposure, no point by point exploration of the spectrum being required, as in the scheme II geometry.

Operation of an instrument of the scheme II geometry requires in principle, that the source be moved along the focal circle, while radiation intensities are measured continuously

by the counter. Source positions corresponding to peaks of measured intensity can be converted to gamma ray energies through the Bragg relation. In practice, to avoid the necessity of moving the heavy collimator and the still more heavily shielded gamma ray detector behind the collimator, the focal circle and source are rotated, while the detector is held fixed in space. Linkages are required to rotate the crystal in order to maintain the correct alignment and to accurately determine the distances and angles involved in the rotation. Flexures of the mechanism require quite complex alignment and compensating devices. A good description of the careful attention to detail required for such an instrument is given in reference (13).

E. INSTRUMENT EFFICIENCY CONSIDERATIONS

An important consideration in estimating the exposure times required for gamma ray measurement is the efficiency of the spectrograph as a function of quantum energy. The efficiency may be defined as the ratio of the number of gamma quanta absorbed in a particular line on the nuclear emulsion to the number of quanta of that energy emitted by the source in all directions.(9) This efficiency is determined by three factors: (1) The acceptance angle around the Bragg angle or the integrated reflection coefficient, R_θ, within which the quartz lattice will accept and reflect radiation from an atom in the source. (2) The distance of the source from the crystal and film holder. (3) The efficiency of the detector placed on the focal circle of the spectrograph.

Lind, West and DuMond(21) have investigated the reflection properties of the (310) planes of quartz over the wave length range 500 to 9 x.u. for the transmission case. They have experimentally determined the value of the integrated reflection coefficient, R_θ. This parameter is the equivalent angular range about the Bragg angle, over which 100 per cent of the photons are reflected in accordance with the Bragg condition. R_θ essentially determines the usable solid angle into which an emitting atom in the source can radiate in order to be selectively reflected by the crystal planes. The variation of R_θ with energy has been derived from the data of reference (21) and is presented in (9) for a 2mm thick crystal as

$$R_\theta = \frac{3.5 \times 10^{-2}}{E_\gamma^{\,2}}$$

where E_γ is the quantum energy in kilovolts, and R_θ is given in radians.

In Figure 6, we have selected an atom in the source. d is the distance from source to crystal, D is the distance from crystal to film (closely 200 cm. in the present case), and h is the effective height of the crystal per 1 cm line height on the film. From the geometry $h = \frac{d}{d+D}$. The solid angle within which all quanta leaving the source will be reflected onto the film is given by

$$\Omega = \frac{R_\theta \, d \, h}{4\pi d^2} = \frac{R_\theta}{4\pi(D+d)}$$

Substituting the empirical relation for R_θ, we obtain a geometric efficiency, η_g, which is the ratio of photons

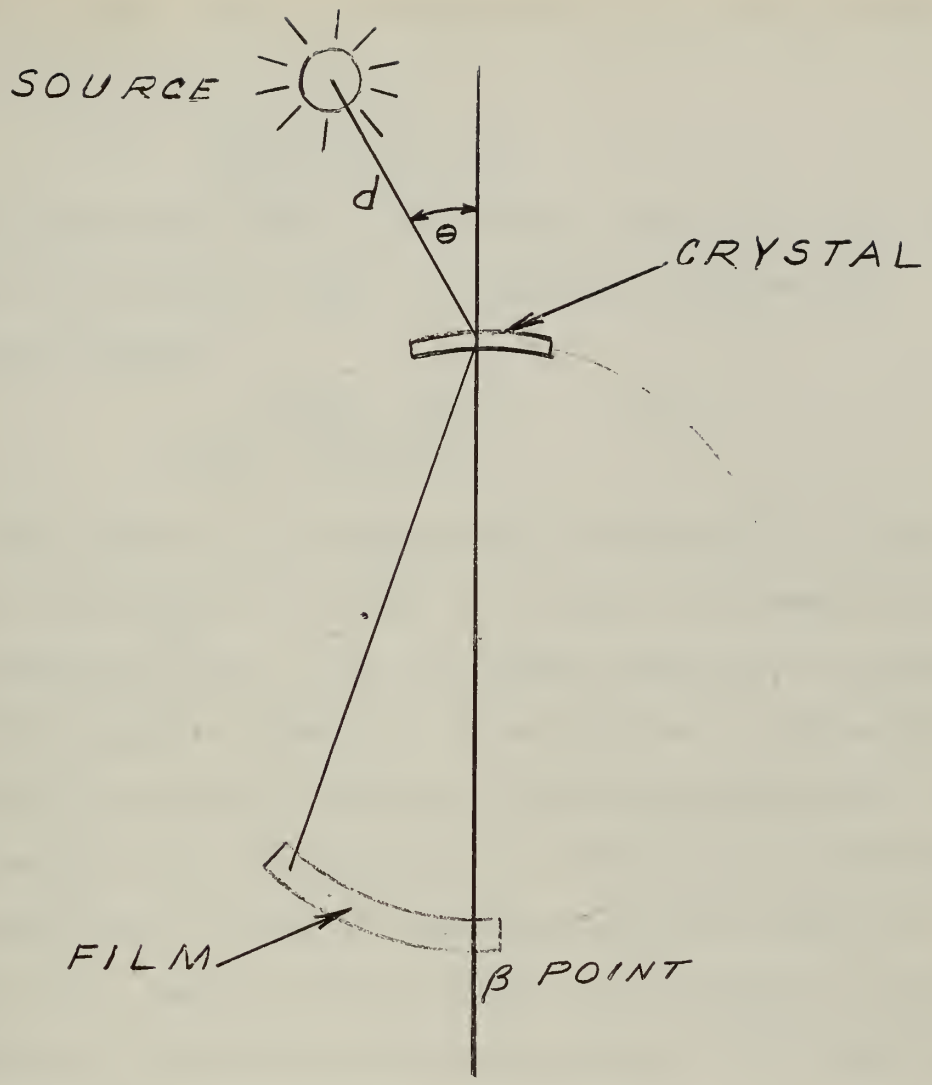

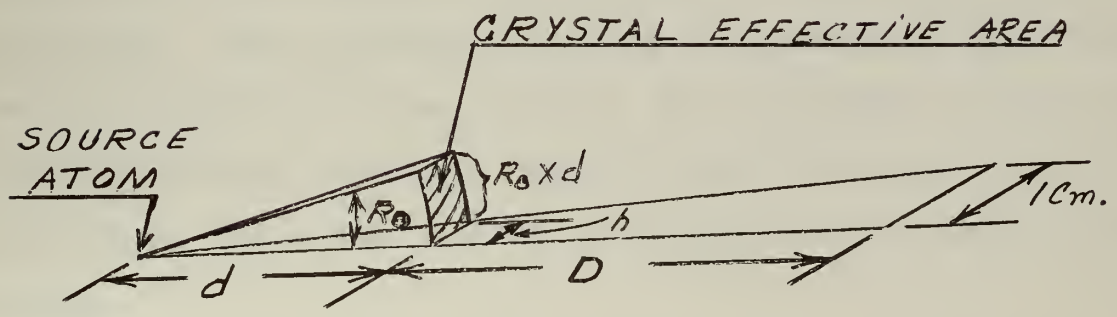

Figure 6

Efficiency - Nomenclature

reaching a 1 cm. line in the detector to the total number of photons emitted by the source.

$$\eta_g = \frac{3.5 \times 10^{-2}}{4\pi(D + d)\, E_\gamma^{\,2}}$$

For the geometries used in this thesis, the film height was 2.54 cm., $D \cong 200$ cm., and $d \cong 100$ cm. The geometric efficiency becomes

$$\eta_g \cong \frac{2.35 \times 10^{-5}}{E^{\,2}}$$

The geometric efficiency must be multiplied by the detector efficiency to obtain the overall instrument efficiency. It is necessary that a high efficiency detector be employed if reasonable exposure times are to be attained. Two efficient detection devices are possible, a scintillation counter behind a very narrow slit arrangement, or a thick nuclear emulsion. The latter type of detector had been used previously at Livermore (7), and has the advantage of exposing all lines simultaneously instead of requiring separate line measurements as with the slit arrangement. For these reasons, the work described in this thesis was carried out using Ilford G-5 emulsions. These emulsions were of a thickness of 600 microns and were mounted on glass plates. The efficiency of 600 micron nuclear emulsion is of the order of 200 times that of no screen x-ray film, which was used in the Hartmann tests with an x-ray machine.

Reference (21) gives an estimate of the efficiency function of the emulsion in the region of a few hundred kilovolts. This estimate, based on the data on emulsions given

by Goldschmidt-Clermont (18) and the gamma ray absorption cross section measurements of Davisson and Evans (10), is:

$$\epsilon = .06 \left[\frac{2.56 \times 10^6}{E_\gamma^{\,3}} + \frac{1}{E_\gamma^{\,1/3}} \right]$$

The total efficiency of the spectrograph is then:

$$\eta_T = \epsilon \eta_g = \frac{1.41 \times 10^{-6}}{E_\gamma^{\,2}} \left[\frac{2.56 \times 10^6}{E_\gamma^{\,3}} + \frac{1}{E_\gamma^{\,1/3}} \right]$$

At a quantum energy of 100 kev the total efficiency is 3.9×10^{-10} while at 300 kev it is 3.9×10^{-12}, which is a decrease by a factor of 100.

The above efficiency analysis still provides no measure of the length of exposure required unless it is known how many photons are required to produce a measurable line on a nuclear emulsion. Reference (21) quotes a rule of thumb of one curie hour of a specific energy transition to produce a line in the neighborhood of 100 kev. Using the derived energy function for efficiency, we would expect 100 curie hours to be required for a line at 300 kev. It thus became apparent early in the experimental work that sources of several curies strength would be required if exposures were to be obtained in reasonable times. Wherever possible, exposures in excess of 50 curies hours were obtained. In one case, that of Ytterbium, an exposure of approximately 200 curies hours was made. It was gratifying to discover that the 396 Kev gamma ray line was of sufficient strength to be measured on this plate.

SECTION III - DESCRIPTION OF EXPERIMENTAL APPARATUS

A. TWO METER BENT CRYSTAL SPECTROGRAPH

Figure (7) is a photograph of the assembled spectrograph with a source in position for exposure. Radioactive sources are placed in the shielded exposure container at the right and a glass backed nuclear emulsion is placed in the film holder at the left. The crystal may be seen to the right of the center. This spectrograph employs a bent quartz crystal 2 mm thick by $3\frac{1}{2}$" long by 3" wide. The crystal has been cut so that the (310) planes are perpendicular to the large surfaces of the crystal. Figure (8) shows the crystal holder with the crystal in it. Section B discusses the crystal and holder in detail.

The authors are indebted to Professor H. Mark of M.I.T. for bending the crystal and for supplying the crystal and crystal holder from previous work at the Radiation Laboratory, Livermore, California. Crystals are easily broken during the bending process but once securely in the crystal holder no further adjustment is necessary.

The lead bricks between the crystal and film holder form a crossover point shield. This shield passes the diffracted rays and blocks out the direct rays from the film. A detailed description of the cross over point is given in Section IV, Part C. The four inch thick lead wall around the source exposure container forms a major part of the biological shield.

Figure (9) shows the film holder of the spectrograph. This film holder is machined to a one meter radius. It is capable of holding film which is 14 inches long by $2\frac{1}{2}$ inches wide. The

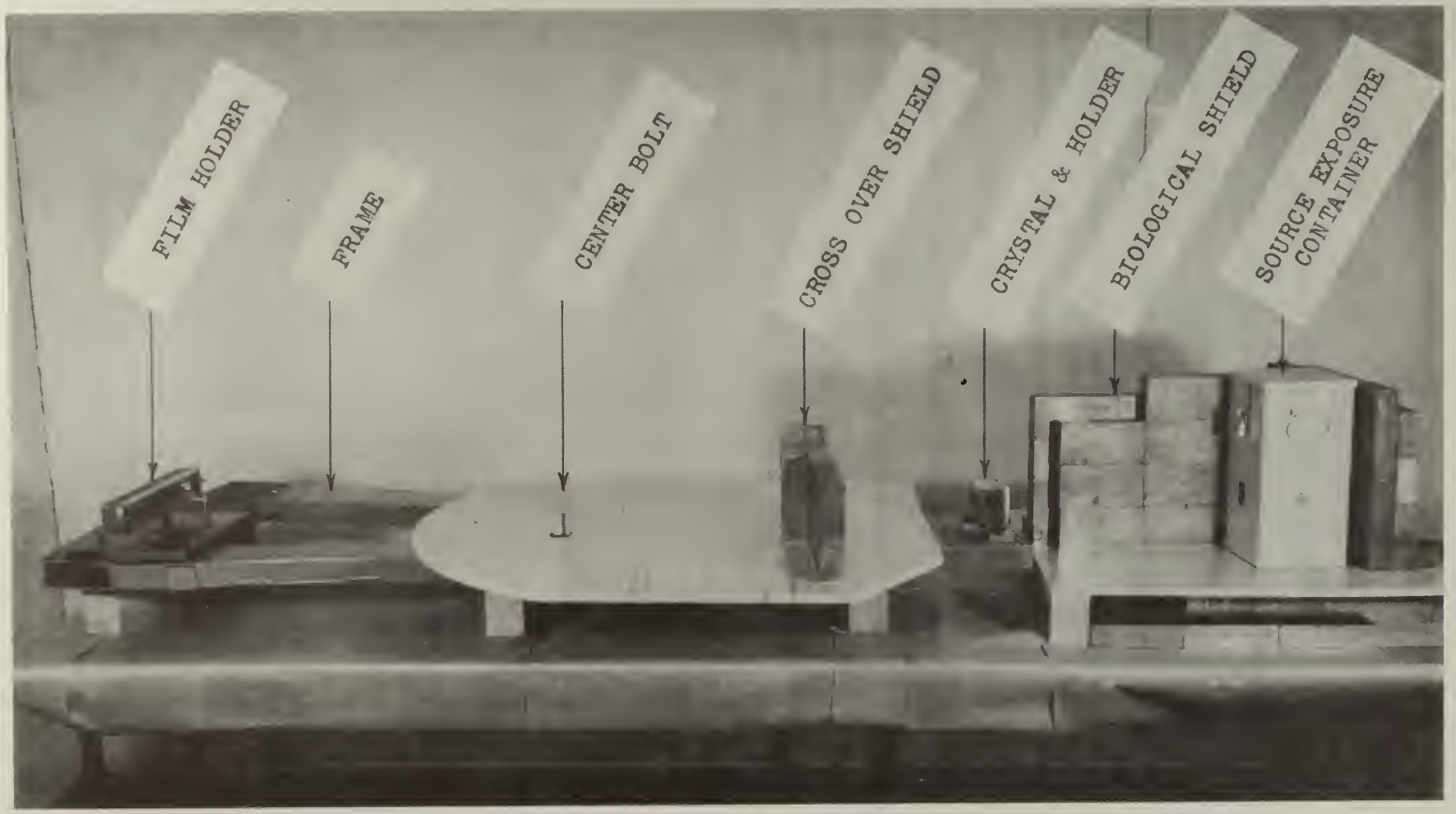

Figure 7 - M.I.T. two meter bent crystal spectrograph, Cauchois type.
Shield wall nearest camera removed for clarity.

maximum useful area of the film is 12 inches long by 1 inch wide.

Basic support for the spectrograph was provided by two drafting tables. Three pieces of wood planed parallel and $5\frac{1}{4}$" X 4" in cross section support the frame on top of the tables. The height of the frame above the table was determined so that two standard 2" X 4" X 8" lead bricks could be used for shielding under the source. This arrangement also placed the film holder and source exposure area at a conveient height above the floor. The assembled spectrograph weighs about three hundred pounds. The lead needed to shield the source adds about 1000 lbs. These experiments were performed in a wooden frame building where floor loading had to be considered. Hence, large aluminum plates were placed under the legs of the drafting tables to spread the load over a larger floor area.

B. QUARTZ CRYSTAL AND CRYSTAL HOLDER

The quartz crystal is clamped between two hardened blocks of stainless steel, shown in Figure (8). The material is a heat treatable stainless stell having the composition Cr 13.5%, C 0.35%, Mn 0.40%, Si 0.50%, selected especially for its thermal expansion coefficient, which matches closely that of quartz in the direction transverse to the optical axis. It is obtainable from Firth-Sterling or Allegheny Ludlum Steel Companies (13). One of the steel blocks has a convex and the other a concave profile to bend the quartz crystal to the required radius of two meters. Only the convex block actually determines the curvature of the quartz since a rubber gasket is placed between the concave steel surface and the quartz plate. The pressure is not applied directly by the screws which pull the two plates together. Instead compression springs are used between the screws and the blocks to lessen the danger of too great a pressure which might break the crystal.

The extremely important techniques involved in profiling and lapping of the stainless steel blocks in the crystal holder are described in reference (16). The quartz slab is prepared from perfect specimens of monocrystalline material known to be completely free from either optical or electrical twinning. Slabs are cut at the correct angle, etched, ground, lapped and polished to optical flatness. Reference (13) contains a summary of this procedure.

C. SOURCE HANDLING AND STORAGE EQUIPMENT

1. General

Experimental work for this thesis was conducted in Room

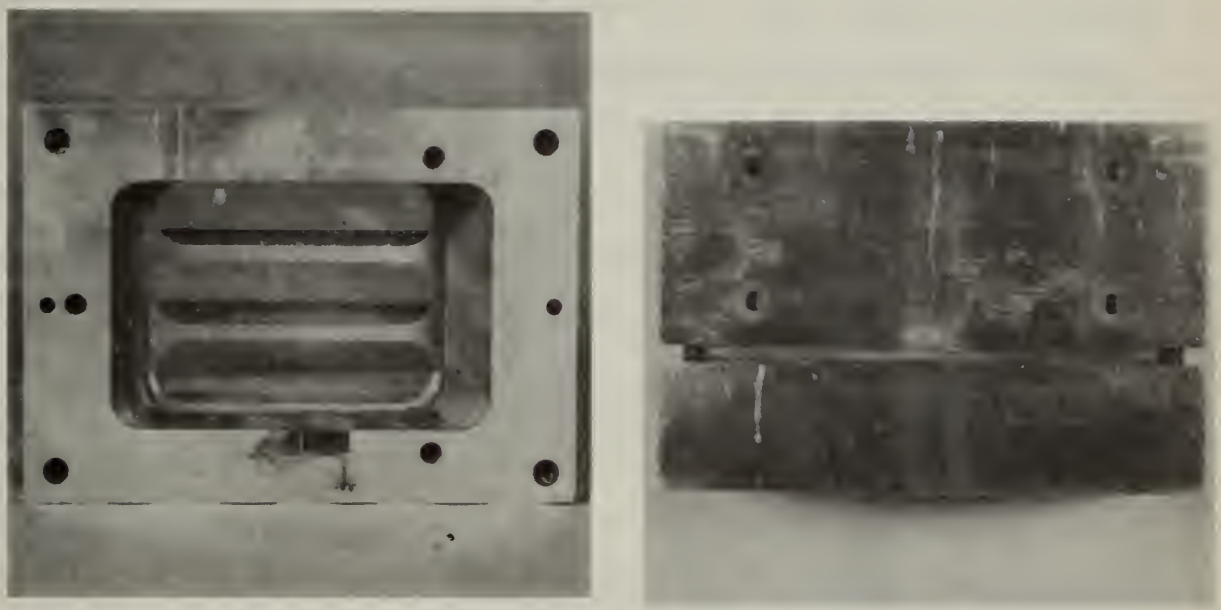

Figure 8 - Crystal holder containing quartz crystal. Left: Front view. Right: Plan view. Note curvature of crystal in plan view.

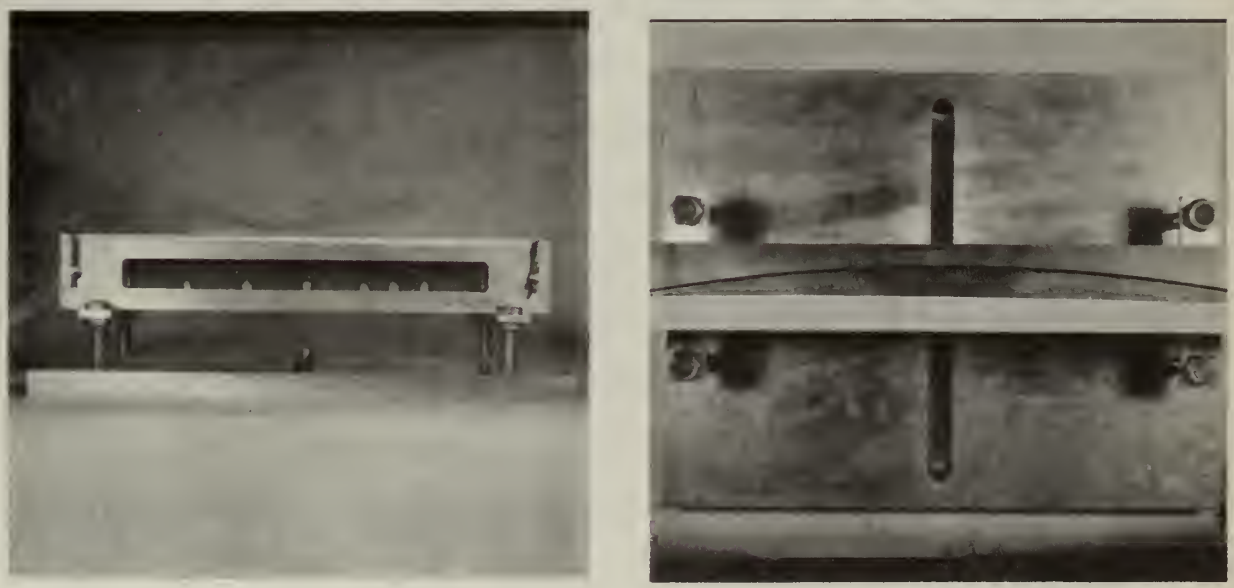

Figure 9 - Film holder. Left: Front view. Note height adjustment screws and lead markers. Right: Plan view. Note curvature of holder and approximate energy scale.

320 of Building NW-12, adjacent to the M.I.T. Reactor, 138 Albany Street, Cambridge, Massachusetts. This area of Building NW-12 is restricted to the use of sealed sources only. Access to Room 320 from the reactor proper requires transit through general usage areas not restricted to personnel normally working with radioactive material. To provide personnel protection and also to insure minimum interference to other experiments, a requirement of 1 mr/hr at 1 ft from the transport container was established as the maximum permissable dose rate during source transportation.

Stringent shielding requirements around the radioactive source are imposed by the location of Room 320. It is directly over a classroom which is in use several hours a day during the academic year. The area on the third floor immediately surrounding Room 320 is a non-restrictive clean area. This location led to the requirement of a dose rate at the boundaries of the room not to exceed .25 mr/hr.

Since it was determined early in the conduct of the thesis that source strengths of several curies would be needed, considerable care was devoted to satisfying of the above dose rate requirements. A significant portion of the time involved in the thesis was spent in designing, fabricating and procuring the source exposure, source handling, and transporting equipment. The design and selection of equipment was made according to the following principles: Each device must accomplish its purpose and yet be

a) simple to operate and reliable in use

b) simple to construct, to conserve time and money.

c) easy to maintain.

Fire and security requirments imposed the condition of having all sources in locked steel containers whenever the room was unattended.

2. Transportation Containers

Shielding calculations were based on assuming a point source giving off gamma rays of 1.33 Mev with one such gamma for each disintegration with a maximum source strength of 2 curies. This combination of source strength and gamma energy was determined to be the most demanding of the shield for this series of experiments. Allowance for a build up factor was made by taking $B = 1 + \mu x$ where μ is the linear attenuation coefficient and x is shield thickness. This is a conservative procedure and was so intended. These approximate shielding calculations determined that about 8 inches of lead would be the maximum thickness shield needed to satisfy the 1 mr/hr at one foot requirement. Floor loading and the lack of overhead weight handling equipment on the third floor were limiting factors in determining total container weight.

Figure (10) shows the finished product. Standard 2" X 4" X 8" lead bricks, staggered to reduce leakage at the brick joints, were wedged in place in a steel box. This box was mounted on a, commercially available, 3000 lb. capacity hand truck. The shielded volume is 2" deep by 4" square. A removable sheet metal tray allows easy decontamination of the shielded volume. To reduce weight, the bricks at the corners farthest

Figure 10 - Source transportation dolly.
Shielded volume, 2" deep by 4" square.
Shield, 8" thickness lead all directions.
Total weight, 2000 lbs.

Figure 11 - Source transportation cylinder returning a source to the top of the MITR for re-irradiation. Shield, 2" thickness lead all directions. Total weight, 200 pounds.

from the source were omitted, i.e. a sphere was approximated as closely as possible using the rectangular bricks. Closure of the access well is by manual insertion of 2 lead bricks bolted together (50# weight). Total weight of this dolly is about 2000 lbs. It has transported singly without exceeding the 1 mr/hr at 1 ft. requirement a 20 curie source of Dyspresium and a 1.85 curie source of Tantalum as well as other sources of lesser strength.

A smaller container was also constructed. It is cylindrical in shape having an outside diameter (less handles) of 7.25 inches. Figure (11) shows this container about to land on the reactor top. This container proved useful in returning decayed sources to the reactor for re-irradiation and also as part of the wipe test equipment on the reactor top. The sling and custom tailored steel pallet were also constructed. Shielding by this container is equivalent to 2 inches of lead. Three inches of lead shielding is achieved with an insert at the expense of reduced shielded volume. This insert was constructed after experience dictated the need. Closure is by manual operation of the 35 lb. top lead disc which is secured by brass clips.

Source insertion into either container is by gravity from a bottom gate opening container placed flush on top of it or manually by squeeze grip tongs. Source removal in both cases is by squeeze grip tongs.

2. Source Exposure Container

A cylindrical lead shield for a Geiger tube was converted to a source exposure container by milling a one inch wide by two and one-half inches long aperture in the cylindrical wall. A

Figure 12 - Source exposure container. Left to right: source, positioning tube, cylindrical lead shield, outer steel box.

Figure 13 - Assembled source exposure container less the outer steel box. Source removal string at right side.

central copper tube (1 1/8" O.D.) was also added. Figure (12) shows a dummy source, the central tube, the cylindrical shield, and the outer steel box. Figure (13) shows the assembled shield with source in place less the steel box. The copper tube serves two functions: It is a source positioning device and also a source removal device. Inner diameter of the copper tube is one inch which allows the source container to slide freely in and out but positions the source to within the wall thickness of the source container. Reasonably exact source positioning is required. (See Section IV, part C). A wooden bottom, rubber padded, to prevent damage to the source container, allows removal of the source by removing the entire copper tube. The tube is centered in the lead shield by two wooden spacers secured to the tube. The shield is 1½ inches of lead on the side wall and 2 inches of lead top and bottom. The whole assembly is placed in the steel box prior to source insertion. After the source is inserted, the box can be locked to provide security. This box is also designed so that if the lead cylindrical shield melts all molten lead will be below the hole in the box. Some measure of source containment is thus provided in event of fire. Usually four inches of additional lead shielding in the form of 2" X 4" X 8" bricks was necessary to meet the .25 mr/hr at the room boundaries. This is visible in Figure (7).

4. Temporary Storage Vault

Figure (14) shows the temporary source storage vault constructed in Room 320. It is simply 2" X 4" X 8" lead bricks arranged in and under a steel box to provide 8" of lead shield

Figure 14 - Temporary storage vault for radioactive sources. Shield, 8" lead all directions. Shielded volume, 2" x 4" x 8". Room 320, Bldg. NW-12, M.I.T.

around a shielded volume of 2" X 4" X 8". Each source has a color coded hole in a wooden tray and when not in use in the exposure container it is stored in this vault. This temporary measure was necessary because the permanent vaults in the M.I.T. Reactor Building have not yet been completed. Insertion and removal of sources from this vault is by squeeze grip tongs with the observer using a mirror permanently mounted above the vault.

D. SOURCE MATERIALS AND CONTAINERS

The rare earth elements used in these experiments were in the powdered oxide form. Natural abundance rare earth oxides 99.9% pure were purchased from Lindsay Chemical Division of American Potash and Chemical Corporation, West Chicago, Illinois. These powders were placed in aluminum containers designed and manufactured by the authors. Considerable time and thought went into the final source container. Details will be given here in the hope that future workers on this project will be saved from traversing the same ground.

Aluminum was chosen as the container material because of its short half life of 2.3 minutes. The volume of material in the container is considerable and results in a strong source of itself. Therefore, it is mandatory that this activity decay quickly unless elaborate hot cell remote handling equipment is available. Commercially available 2S aluminum is suitable except that its machinability is poor. It was found that 6063 aluminum although containing a small amount of Silicon was satisfactory and the machinability was much better than 2S. One inch diameter round stock of 6063 aluminum was purchased as the raw material.

A sample of the bar was irradiated and the activity checked to determine the half-life. This procedure is recommended for each new piece of stock purchased from a commercial supplier. It avoids wasting time making up containers from material nominally correct but actually containing objectionable impurities.

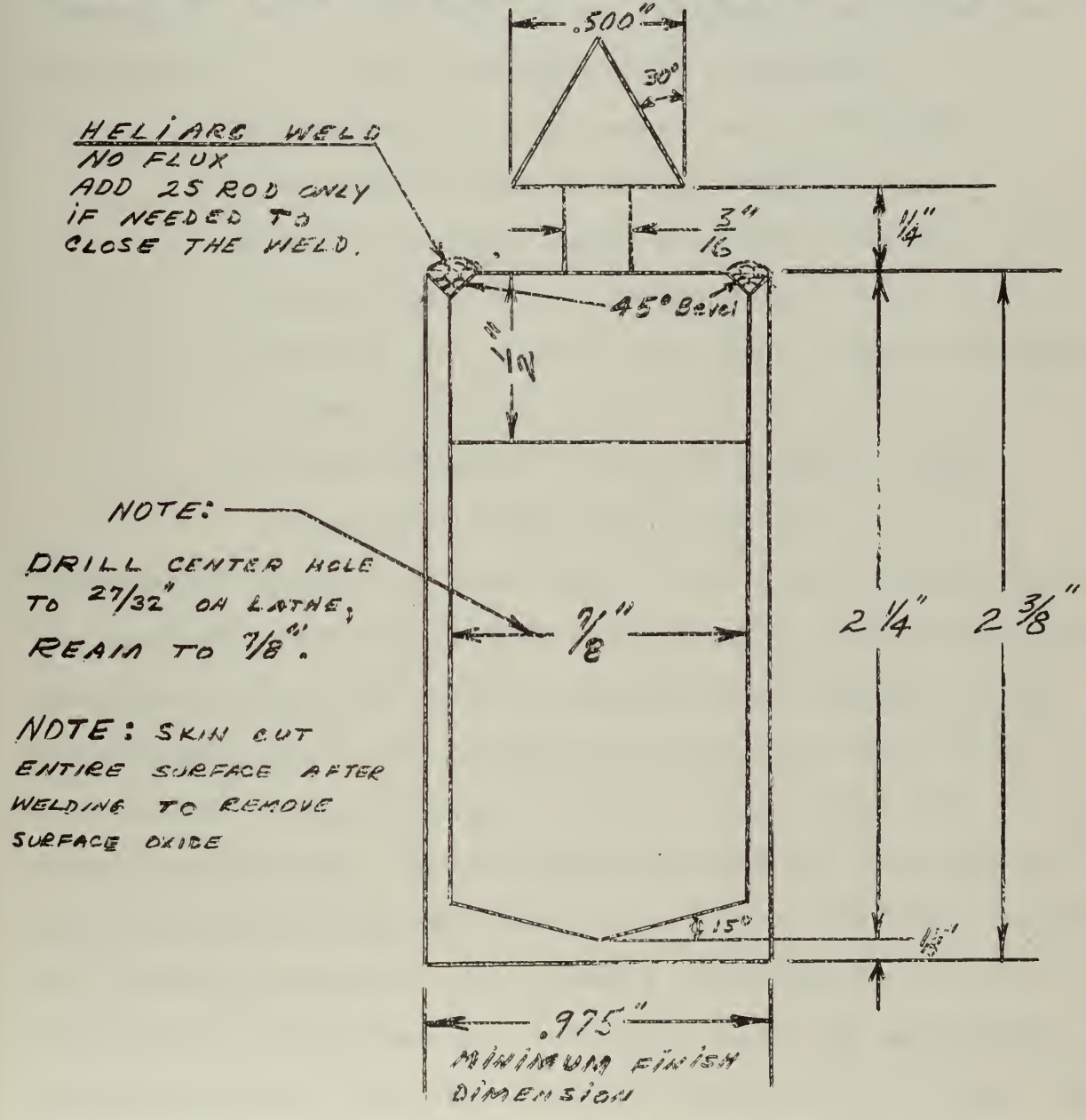

Figure 15
Cross Section of Sample Container

Figure 15 is a scale section of the source container.

Maximum container diameter was limited to a size which would freely pass through the vertical irradiation facility available in the M I T R. Maximum container length was determined by the useful height of the crystal and also by free passage through the curved portions of the vertical irradiation facility in the M I T R. These two lengths are compatible.

The manufacturing processes are as follows:

1) Cut round stock in 2 3/8" lengths.
2) Drill and ream inside as shown in Figure (15).
3) Machine 45° bevel on open end.
4) Machine the top hat from round stock to dimensions shown in Figure (15).
5) Finish diameter of top hat plug for .001" interference fit with container.

The matched pair of one open end cylinder body and one hat plug are now ready to be thoroughly cleaned inside and out with soap and water followed by several cleanings with acetone. When thoroughly cleaned, the desired source material is placed in the body and the plug is pressed in with a hand press until it is flush with the body. Accurate determination of the amount of material in the container was made by before and after weighings on a chemical balance. The V groove remaining on the top of the cylinder edge is sealed with a heliarc weld with no material added except possibly a small amount of 2S aluminum rod to close off the weld. No flux is permitted because of the impurities which would be introduced in the weld zone. This weld was done with the bottom 3/4 of the sample immersed in water. This reduces

the temperature of the interior during welding and thereby lessens the amount of air forced out of the container during welding. The most troublesome part of the welding process was that of closing the last portion of the bead. Escaping air, heated by the arc, had a tendency to cause pin hole leaks in this part of the bead. Immersing the sample in water while welding was found to provide the necessary cooling to avoid this difficulty.

After welding, the sample is returned to the lathe and a finishing cut is made all over except across the weld bead on the sample's top. This results in a bright, smoothly surfaced sample, easy to clean and easily decontaminated if necessary after irradiation. To absolutely guarantee a gas tight sample, each completed unit is suddenly immersed in water at 90° C. and held there for 20 minutes. This test revealed pin hole leaks in welds during the trial and error period when different container designs were being tried out. The sample is irradiated at a temperature of 60° C. when the M I T R is operated at 1 Megawatt. Figure (17) shows a finished container ready for irradiation.

The staff of the M I T R have developed a gas tight container by crimping the cap to the body. This type container is recommended for source materials which cannot stand the high temperatures of the welding procedure.

An early design which proved not to be gas tight was made by screwing aluminum plugs into aluminum (6063) pipe. Even though pipe threads were used and the ends of the plug machined

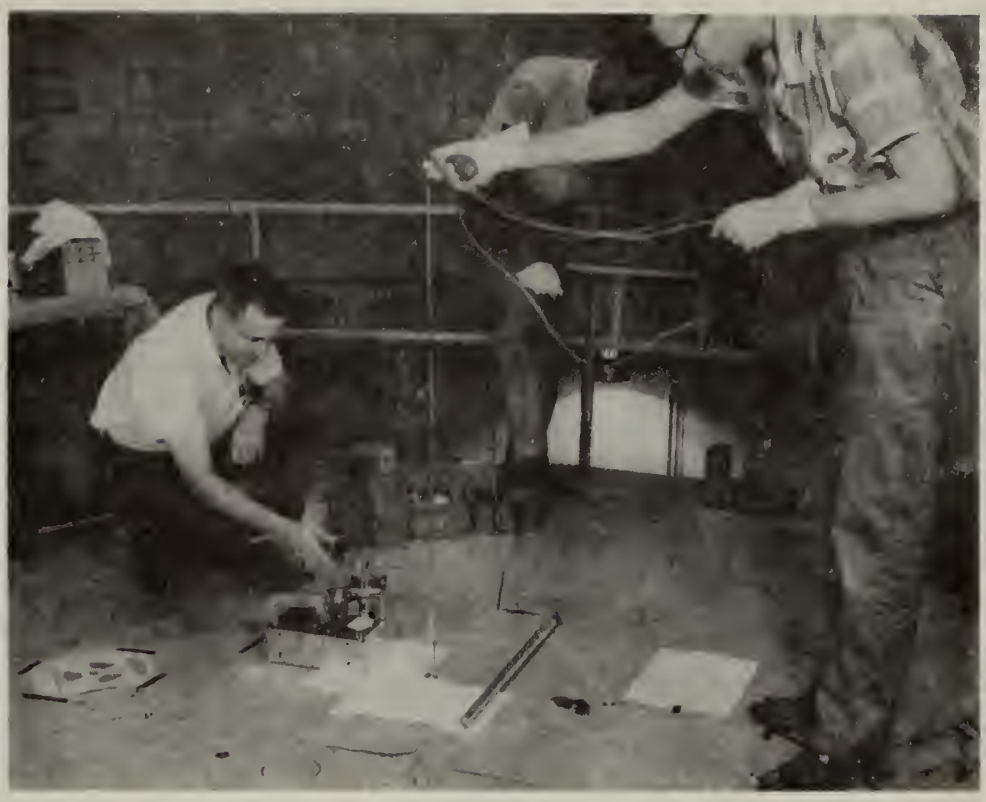

Figure 16 - Inserting a sample to be irradiated in vertical facility of the MITR. Photograph taken on the reactor top.

Figure 17 - Finished sample container ready for irradiation.

off flush, this design consistently failed the hot water test. Bubbles of escaping air could be seen at various places around the thread joint.

E. SOURCE IRRADIATION FACILITY

Sources for these experiments were made in the M I T R. Reference (24) gives a description of the M I T R. Figure (16) shows the method of inserting a source in one of the vertical irradiation facilities. The vertical irradiation facilities are located in ports 3GV5 and 3GV6 of the M I T R. Figure (18) is a schematic drawing of a vertical irradiation facility purchased for this project and currently in use in 3GV6. This facility was designed and manufactured by the M I T R staff. These vertical irradiation facilities are essentially shielded accesses to the inner reflector region of the reactor near the core tank where the flux level is about 5×10^{12} neutrons/ cm^2-sec when the reactor is operated at a power of one megawatt.

Sources requiring irradiations of more than 20 minutes or so are usually irradiated in the vertical facilities. Pneumatic rabbits are available for short time irradiations but were not used in these experiments.

The handling tool for inserting and removing the sources was designed and manufactured by the M I T R staff. It is composed of 2S aluminum, nylon and tygon tubing. The gripping device is pneumatically operated by the squeeze bulb at the end of the tygon tubing.

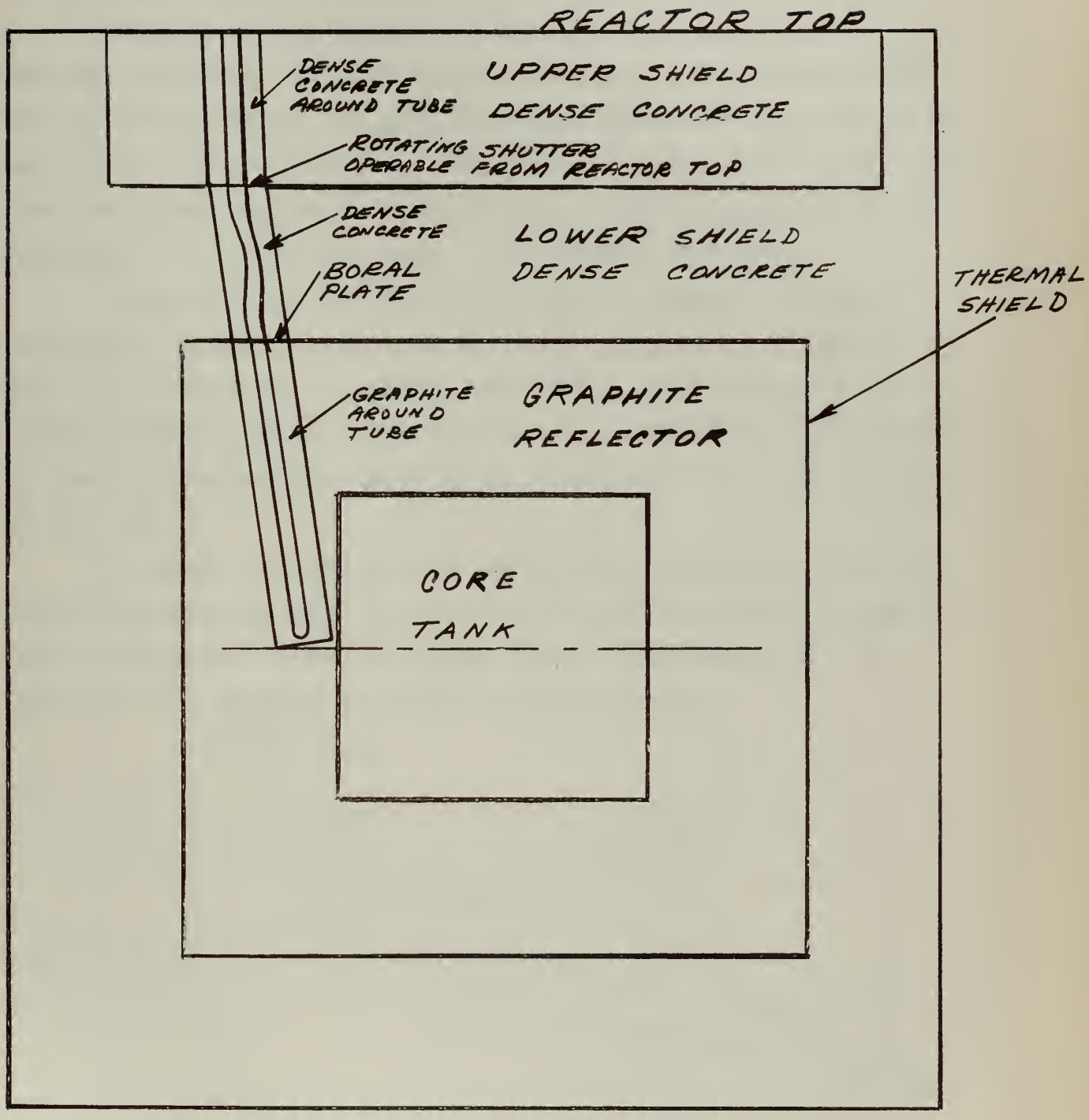

Figure 18

Schematic Diagram Showing Location of 3GV6 in the M.I.T. Research Reactor

SECTION IV - EXPERIMENTAL PROCEDURES

A. OPTICAL ALIGNMENT OF THE SPECTROGRAPH

Purpose of the optical alignment procedure is to provide reference lines by which assembly of the spectrograph may be accomplished. It provides assurance that the assembled unit will be ready for final alignment without undue time being spent on final alignment adjustments. Final alignment is made by means of the Hartmann test to be described later.

Figure (19) shows the spectrograph frame. Machined surfaces A, B and C were checked with a carpenter's level. A and B were found to be in the same plane, but surface C was slightly twisted with respect to A and B. Vertical adjustment of the film holder was later used to correct for the twisting of the frame.

In order to establish a centerline compatible with the crystal holder mounting block, bolt holes in surface B, and the slot in surface A, the following steps were necessary. A telescope was mounted as shown in Figure (20).

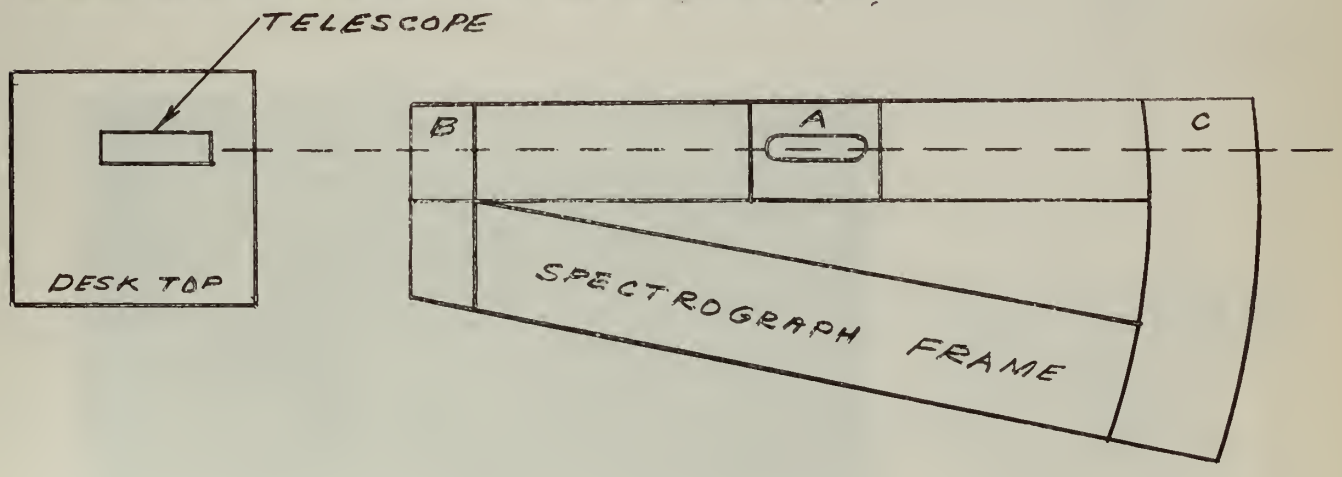

Figure (20) Positioning of telescope for Optical Alignment

Figure 19 - Spectrograph frame, standing on edge to minimize distortion due to camera angle. Machined surfaces A, B, C are labeled. Reference lines for repositioning the cross over point shield platform are seen between A and C and A and B.

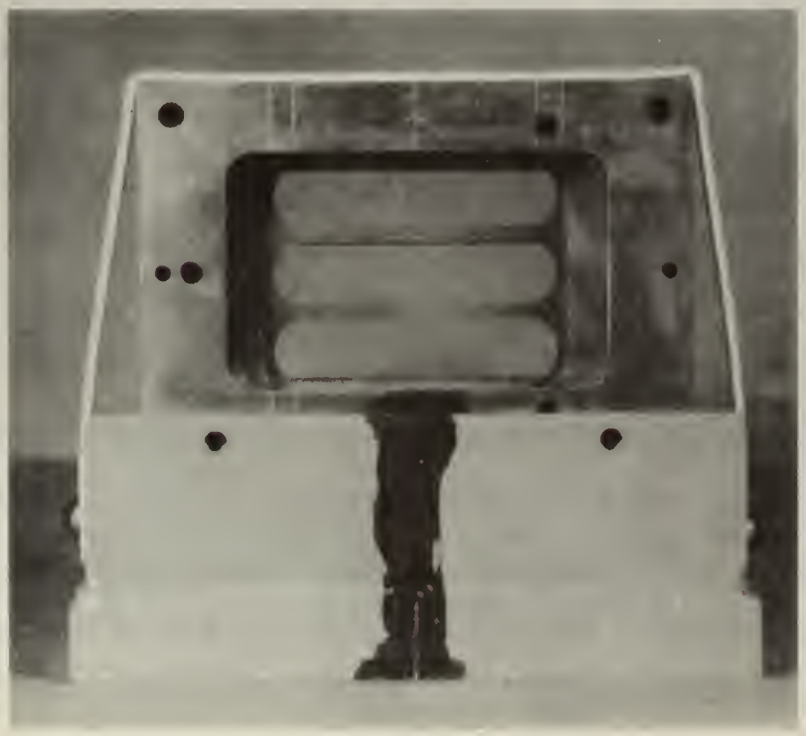

Figure 21 - Crystal holder, centered in and secured to the crystal holder mounting block, looking from source toward film.

The telescope was leveled to swing in a plane parallel to surfaces A and B. The crystal holder was centered in the crystal holder mounting block as in Figure (21). Centerline scribe marks had been provided, front and back, on the crystal holder during its manufacture. Using the front face reference marks, a centerline was scribed on the front edge of the crystal holder mounting block by means of a steel square and scriber. Figures (22) and (23) show the crystal holder mounting block. The crystal holder was then removed from the mounting block and the mounting block was bolted to surface B. Care had to be used to center the mounting block with respect to the tapped holes in surface B. A scribe mark into surface B was placed at the junction of the mounting block centerline and surface B. The mounting block was then removed from surface B.

Next, the telescope was positioned left and right until the vertical cross hair passed through the mark on the front edge of surface B and the center of the slot in surface A. We have now established a vertical plane which is perpendicular to surfaces A and B and which passes through the center of the slot in surface A and which will also pass through the center of the crystal holder mounting block when it is mounted on surface B. The telescope position was not changed during the remainder of the optical alignment procedure.

Focusing of the telescope on each machined surface and separate focusing of the cross hair on the same surface was possible with the telescope unit used. This arrangement permitted very accurate positioning of a steel straightedge parallel to the telescopic line of sight. Allowance was made

Figure 22 - Crystal holder mounting block, plan view.

Figure 23 - Crystal holder mounting block, front view.

for the thickness of the scriber used. Thus, the permanent reference centerline of the spectrograph was scribed into surfaces A, B and C using machinist blue for contrast. These lines are visible in Figure (19).

A check was now made to insure that the vertical plane passed through the center of the crystal holder. This was done by bolting the crystal holder mounting block to surface B using the established lines as references. Next the crystal holder was secured to the mounting block using the established lines as references. It was found that the telescopic vertical cross hair fell exactly on the centerline of the crystal holder. However, there was no assurance that the plane through the crystal holder vertical faces was perpendicular to the vertical plane of the cross hair. In order to provide this and as a positive alignment check the crystal holder and mounting block were reversed as a unit and remounted to surface B using the established lines (now on the face away from the telescope) to position the unit. The telescope was then used to extend the crystal holder centerline to the mounting block back face.

Next the crystal holder and mounting block were removed and remounted in the forward direction. It was found necessary to ream the holes in the mounting block to line up front and back with the line on surface B. After this was done, alignment to surface B was attained.

The film holder was now placed on surface C and leveled by means of the adjustment screws. This insured that the film or emulsion in the holder would be parallel to the crystal.

Center of the focal circle was found by using a large beam compass set to 1 meter distance and measuring back from the neutral axis of the crystal as mounted on surface B. A bolt was placed in the slot in surface A and the center punched in the bolt head. Rough positioning of the film holder was obtained by swinging the beam compass from the bolt center and requiring the film holder to conform to the arc swept by the compass. Further refinement of the film holder position was attempted by the following two means:

1) Line light source method

A line light source was placed on the focal circle about 15 cm to the virtual image side of the spectrograph centerline. In a darkened room the image of the line source reflected from the surface of the quartz crystal is visible on white paper. The paper was moved toward or away from the crystal until the observer picks the position of best focus. The film holder is then moved to conform to the new focal circle. It was found that different observers differed by as much as a centimeter in choosing the position of best focus.

2) Beam compass method

The crystal holder used in this spectrograph had been in use previously at the Radiation Laboratory, Livermore, California. Calculation of an average value of the radius of curvature was possible from the data of reference (9). Using the bolt secured in the slot of surface A and a beam compass setting determined as the calculated average value of the focal circle radius, measuring along the spectrograph centerline from the neutral axis of the crystal fixes the new center of the focal circle. The new center was scribed into the bolt head. Swinging

the beam compass from the center, permitted adjustment of the film holder to conform to the focal circle.

The spectrograph is now ready for the Hartmann tests. Approximately two complete working days were spent on an optical alignment. This is considered a maximum because the sensitivity of the Hartmann test is much greater. Hence final alignment is the result of the Hartmann Test and rough alignment only is required of the optical alignment procedures.

B. HARTMANN TESTS

The most significant alignment check of the spectrograph is the "Hartmann" test. This name comes from reference (11) and is taken by analogy with the Hartmann method of testing the aberration of focus of large astronomical mirrors. The purpose of the Hartmann test is twofold. It determines the line width due to residual imperfections of the crystal plus curvature of its neutral axis and also the amount and direction of movement of the film holder required to reach the point of best focus.

Basically, the Hartmann test measures the difference of line position from various segments of the crystal. This is accomplished by shielding the crystal so that only a given segment of it is used in any one source exposure. Likewise, the film is shielded to record the lines from only one segment at a time, while reserving the shielded part for exposure to the segment of the crystal chosen arbitrarily as the reference segment.

A portable x-ray machine known as the "Hot Shot", manufactured by Picker X-ray Corporation, was used as the source during these tests. The $K\alpha_1$ and $K\alpha_2$ x-ray lines from the tungsten target were focused by the crystal. Due to the large effective source strength of this machine, no screen medical x-ray film could be used for detection. A lead shield which blanked out all but one-fourth of the crystal was used to select the crystal segments. Lead shields machined from 1/4" lead plate permitted exposure of the film in 1/4" horizontal strips. (Figure (24) shows the designations of crystal quadrants and associated exposed film sections.)

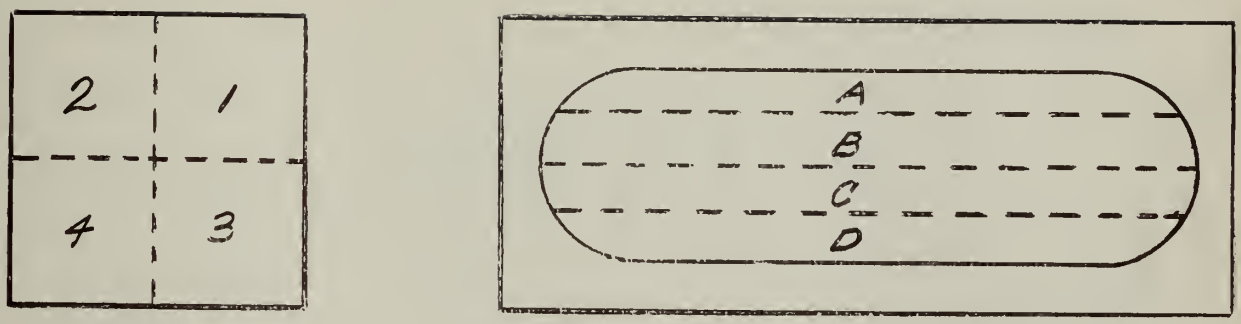

Figure (24) Left: Crystal Quadrant Designations Looking From Source Toward Film. Right: Film Section Designations. A Was Exposed To Rays From 1, B From 2, Etc.

Differences in line position in the four film sections were read by means of an optical comparator. Section A from quadrant was arbitrarily picked as the reference and the differences from A plus or minus were determined from the comparator readings.

Figure (25) depicts the method used for reducing the Hartmann test data to values which can be plotted on a reasonable size plot. The pie shaped pieces formed between a ray and a focal circle diameter through the center of the crystal were approximated by triangles. This introduces negligible error because the arc lengths approximated by cords are very small compared to the radius of the circle. Distance a is 1/4 of the effective crystal width and equals 19.0 mm. Distance b is determined from the comparator readings of the Hartmann test film. When optical alignment, as described previously, precedes the Hartmann test, distance b will be very small. In this case,

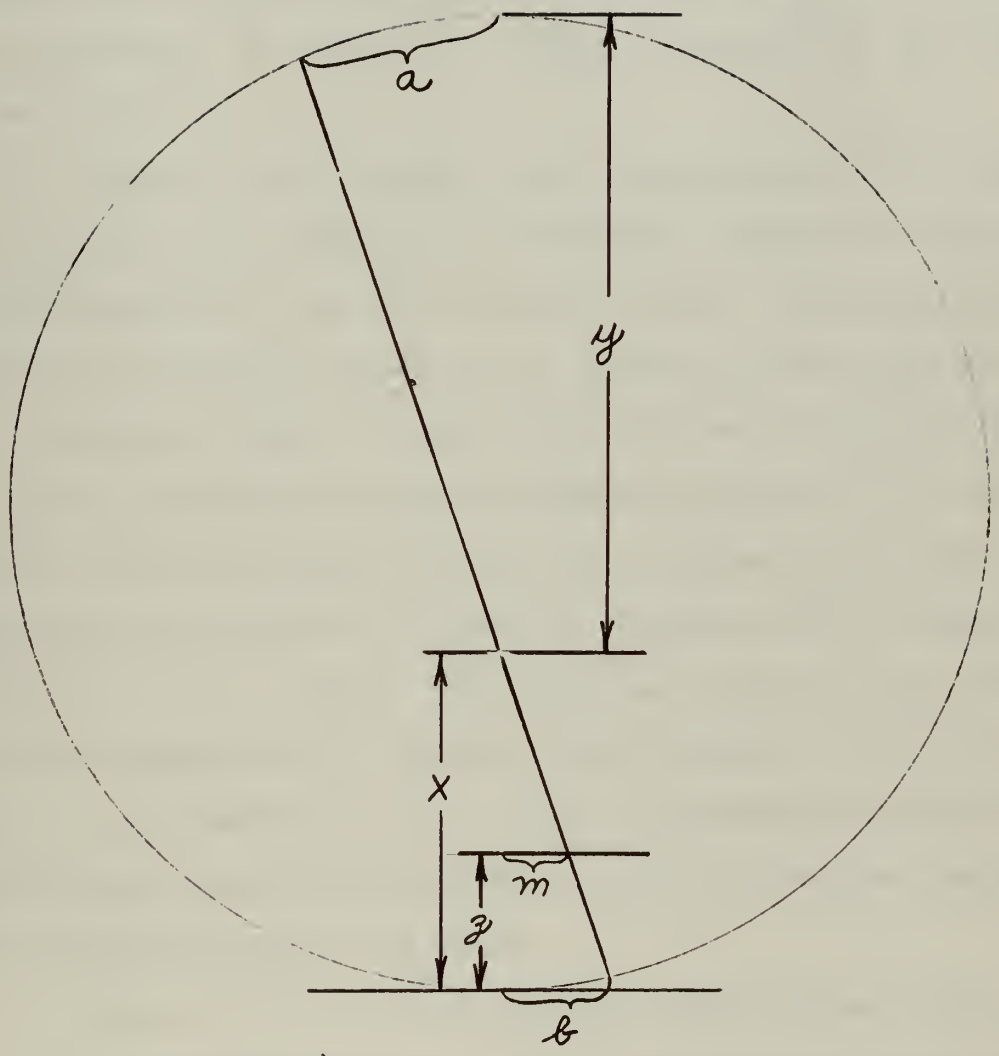

$$m = b - \frac{z\left(1+\frac{a}{b}\right)b}{2R} \qquad x = \left(\frac{b}{a}\right)y$$

$$m \approx b - \frac{za}{2R} = b - .478\,mm. \qquad x + y = 2R$$

WHERE $z = 50\,mm.$, $a = 19.0\,mm.$ $\qquad \frac{m}{b} = \frac{x-z}{x}$

Figure 25

Determination of Distance m for Plotting
Hartmann Test Data

b was $<$ .11 mm. Therefore, the ratio a/b is large, of the order of 200. Hence, (1 + a/b) is approximately a/b. Distance z was chosen arbitrarily as 50 mm for plotting convenience. Distance m is found from similar triangles and, to the accuracy obtainable in the plotting, it equals $(b - \frac{za}{2R})$, where R is the radius of the focal circle.

Figures (26) and (27) show the results of the first and last Hartmann tests conducted. From the comparator readings, the differences AC, AB, AD were determined. These were then converted to distances from a line midway between the extreme rays. In these tests, it was midway between A and D. These values of b are plotted on a horizontal scale of 1" = .05 mm. Next we calculate values of m for each ray and plot these to the same horizontal scale at a vertical distance of z = 5 cm from the points A, B, C, and D. The vertical scale is 1" = 250 mm. The plot is completed by drawing lines 1A, 2B, 3C, and 4D. The region of least aberration of focus is determined and also the direction and amount of movement of the film holder needed to reach the position of best focus.

Figure (26) revealed that the film holder should be moved 1 cm toward the crystal. This was done and the Hartmann test repeated. This procedure was followed until the test results indicated that the film holder should be moved 1.5 mm. This is the same order of magnitude as the thickness of a 600 micron nuclear emulsion mounted on a glass backing plant and wrapped in light tight envelopes. We also found that the 1.5 mm indicated movement was oscillatory. Every other test indicated movement in the opposite direction from the previous adjustment. Figure (27) shows the results of the fourth and

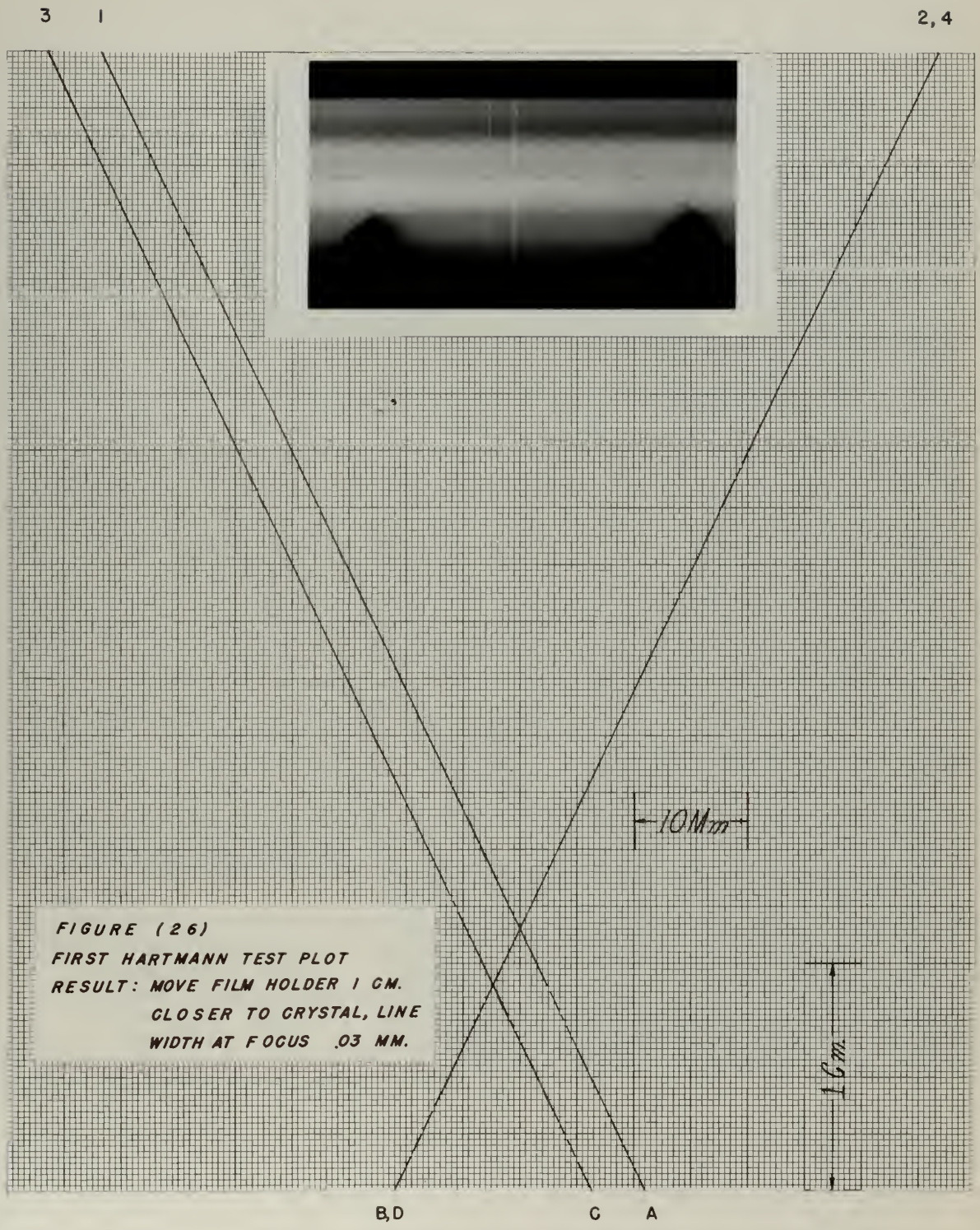

FIGURE (26)
FIRST HARTMANN TEST PLOT
RESULT: MOVE FILM HOLDER 1 CM. CLOSER TO CRYSTAL, LINE WIDTH AT FOCUS .03 MM.

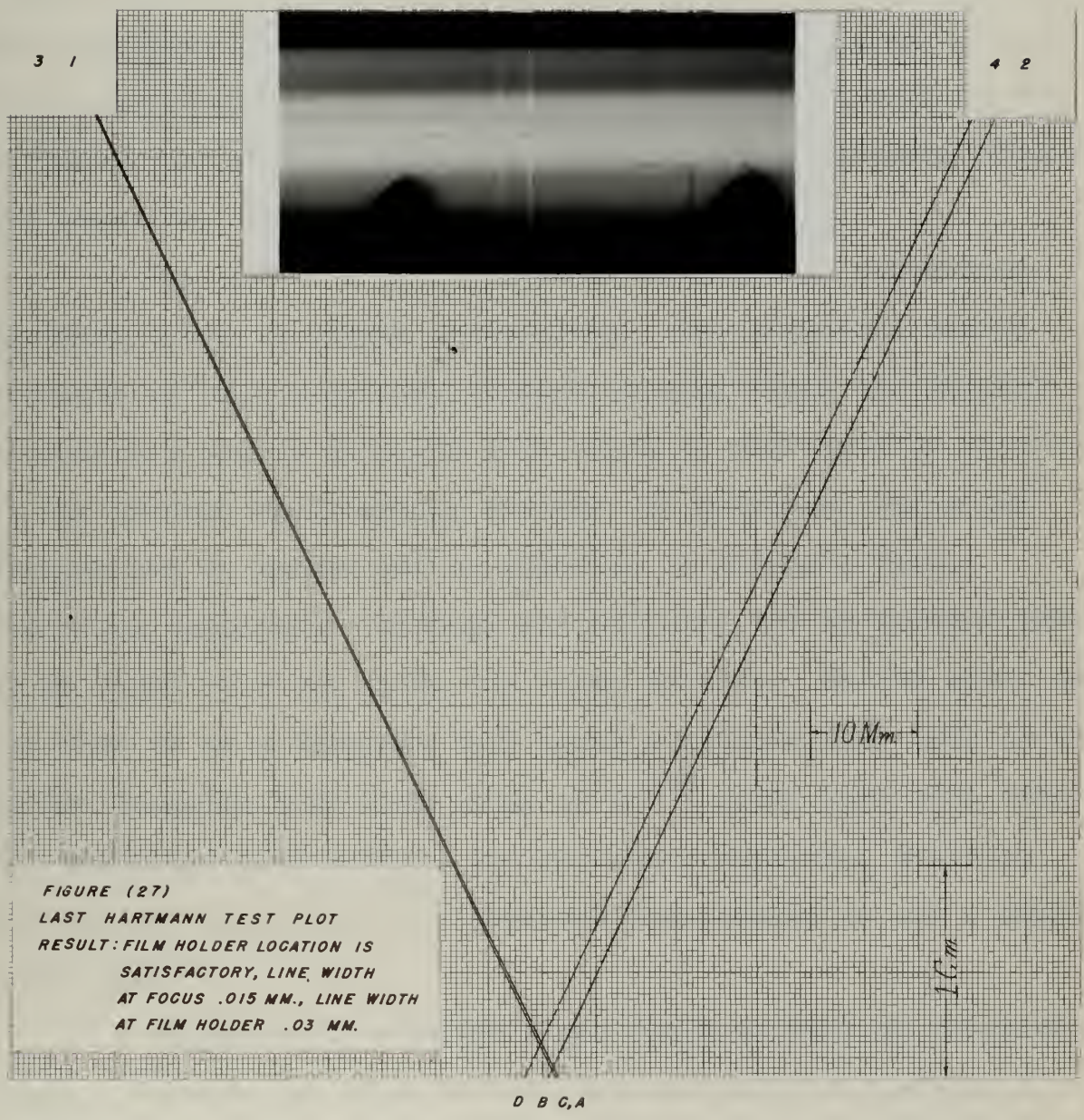

FIGURE (27)
LAST HARTMANN TEST PLOT
RESULT: FILM HOLDER LOCATION IS SATISFACTORY, LINE WIDTH AT FOCUS .015 MM., LINE WIDTH AT FILM HOLDER .03 MM.

last Hartmann test conducted. This plot indicates a width at best focus of .015 mm and width at film position used of .030 mm. The authors were fortunate to have a crystal and crystal holder which achieved a line width due to residual crystal imperfections and curvature of the neutral axis of .03 mm. compared to a value of .05 mm reported in reference (11). Upon completion of the Hartmann test number 4, the spectrograph was considered aligned and ready for use.

The use of a portable x-ray machine for conducting Hartmann tests is highly recommended. The effective source strength of such a machine exceeds by many times the largest radioactive source strength that could be conveniently handled in the present experimental set-up. In addition, the x-ray machine can be turned off as desired. A complete test, including comparator readings and plotting can be accomplished in an eight hour day using the x-ray machine. On the other hand, the time to do a Hartmann test using a nuclear line such as the 68 Kev tungsten line from decay of Ta^{182} would take much longer (of the order of 2 weeks), due to source handling, emulsion processing, and additional exposure time needed to get a measurable line.

Figure (26) revealed slant lines as well as vertical lines. However the slant lines appeared only in quadrant 2, The angle of divergence was measured and found to be about 9°. These lines come from the (932) planes in the crystal. The calculated angle between ($\bar{3}10$) and (932) planes is 9° -03'. Also the spacing between the lines corresponds to (932) reflection. The second quadrant is the only one in which the

Bragg condition was satisfied for the (932) planes. To prove conclusively that the slant lines come from other planes and not stacking faults in the crystal, a series of films were made using the x-ray machine. These are shown in Figure (28). Note that the slant lines can be made to disappear or even change sides by changing the vertical position of the source relative to the crystal, i.e., not satisfying the Bragg condition for the additional planes or doing so for the symmetrically opposite member of the family. Also note that a second set of slant lines appeared at 17°; these are due to the (934) planes.

Published photographs in reference (9) also show slant lines but no explanation is given in that article. It is most probable that these lines are due to refraction from planes other than (310).

By aligning the center of the source at the center of the crystal in the vertical direction, the authors were able to avoid slant lines appearing on the emulsions.

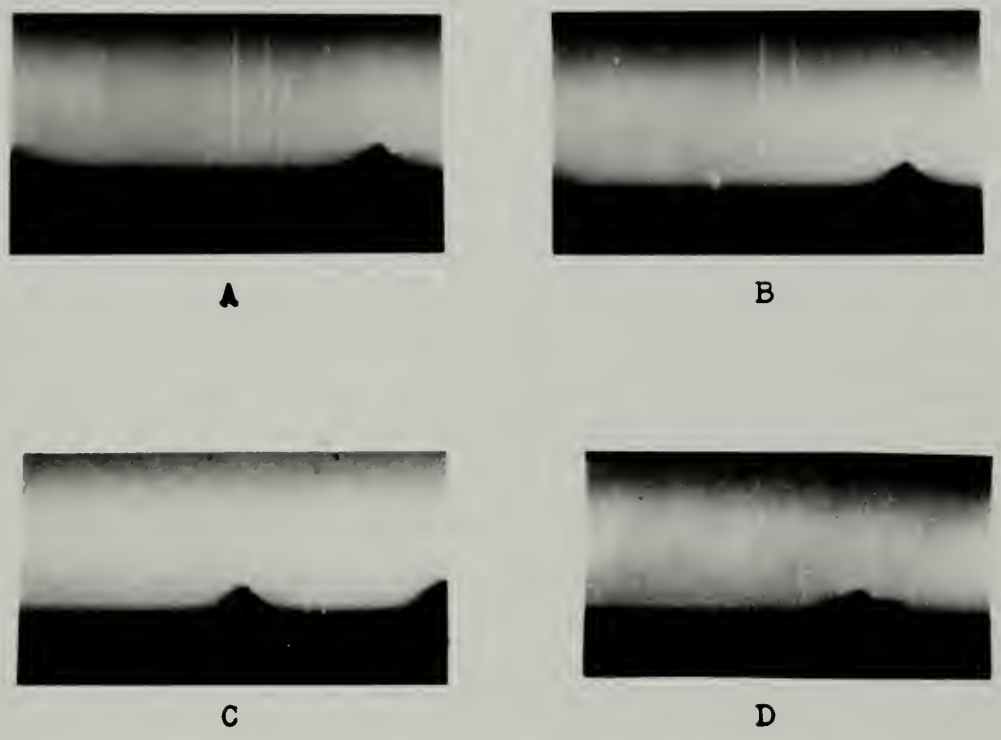

Figure 28 - Slant line study on No Screen x-ray film.

A. Full crystal used with 30 milliamp-minute exposure, using portable x-ray machine. Head lower than crystal mid-height, 1° up tilt on machine. Note slant lines to right, from (932) planes.
B. 3/4 of crystal used, quadrant 2 shielded, with 30 milliamp-minute exposure. Head of machine positioned as in A. Note absence of slant lines from (932) planes.
C. 3/4 of crystal used, quadrant 2 shielded, with 30 milliamp-minute exposure. Head lowered 1 1/4" from position used for A and B. Note that slant lines from (932) planes have reappeared. Also seen are lines from (934) planes. Vertical lines from (310) planes are absent.
D. Full crystal used, 30 milliamp-minute exposure. Head raised 3 1/4" from position used for C. Note slant lines to left from (932) and (934) planes as well as faint vertical lines from (310) planes.

C. SOURCE POSITIONING AND SHIELDING

1. Source Positioning

The source must be positioned so that the desired band of gamma ray energies will be selectively diffracted to the emulsion, while at the same time, the emulsion is shielded from the direct rays. The positioning is always a compromise between three restrictions:

(a) High energy limit, determined by the crystal not seeing all of the source on the high energy side of the crystal.

(b) Low energy limit, determined by the crystal not seeing all of the source on the low energy side of the crystal.

(c) Direct beam blackening of the emulsion in the energy range of interest.

"Seeing" in the present context is taken to mean that gamma rays from the source strike somewhere on the crystal surface at the required Bragg angle.

Directly from the Bragg Law, it is clear that the lower energy rays will be diffracted through larger angles than higher energy rays. We may define the low energy side of the crystal as being the side of the crystal in which the largest Bragg angle is possible for a given source position. Similarly, we may define the high energy side of the crystal as being the side in which the smallest Bragg angle is possible for a given source position. In figure (29), the low energy side is the left side and the high energy side is the right side of the crystal. In the Cauchois geometry, with an extended source, the low energy

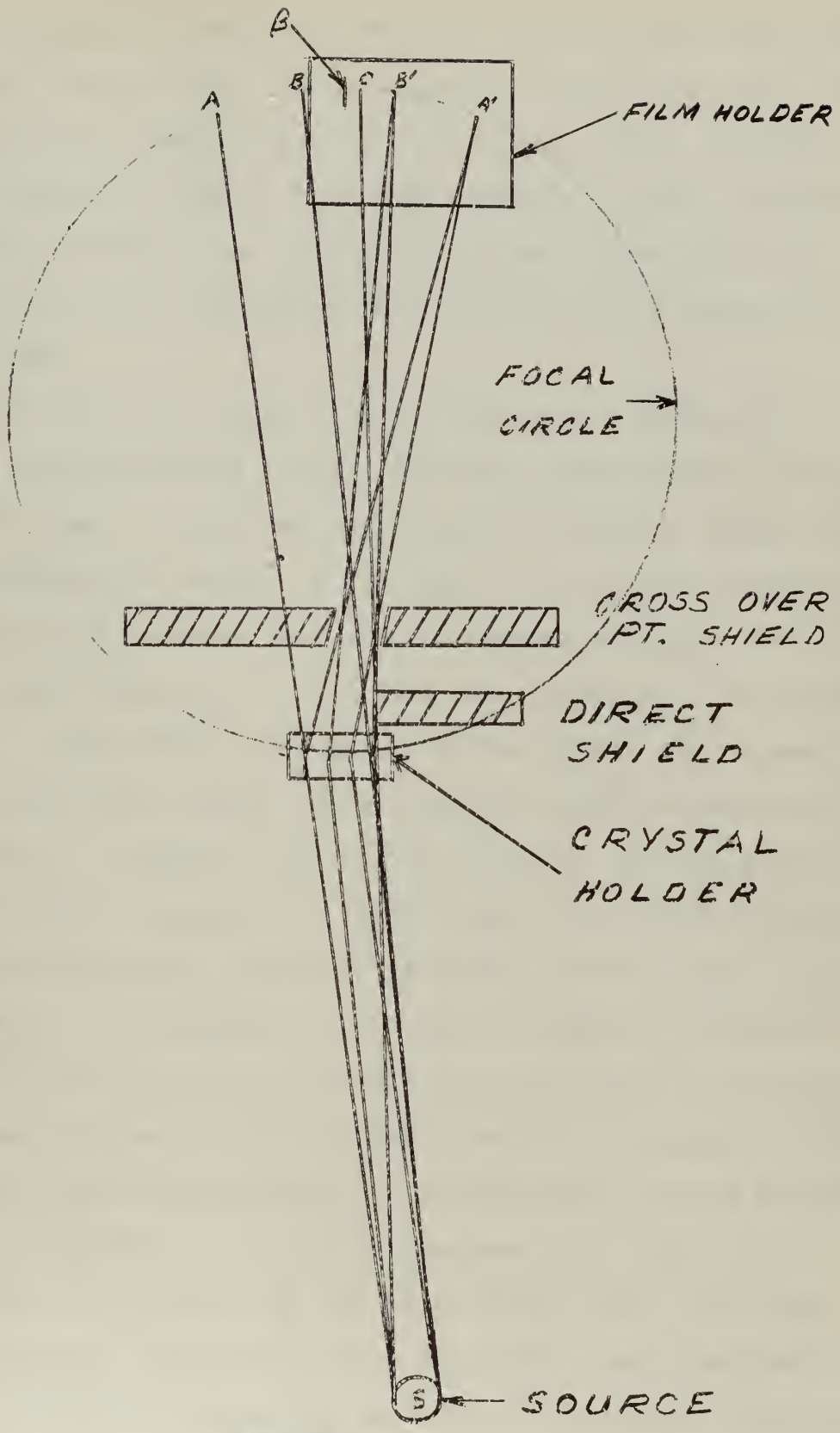

Figure 29

Source Positioning

rays are focused in positions further to the right on the film than higher energy rays. It is apparent from Figure (29) that the high and low energy rays must cross each other somewhere between crystal and film. Here the bundle of rays is about the same width as the source. A shield placed at the cross over point will pass the diffracted rays and block the direct rays from the film.

In determining where to position the source, the following considerations apply. It can be seen from a study of Figure (29) that the high energy cut-off is raised on the energy scale by moving the source to the left. On the other hand, such a movement would increase the amount of blackening of the film by direct radiation, and at the same time raise the low energy cut-off. If the source were moved to the right, the direct radiation and lower energy cut-off limits would be improved at the expense of a reduced high energy cut-off. Movement away from the crystal in general slightly helps the direct blackening limit, but reduces the spread of energies between high and low energy cut-off. Instrument efficiency is reduced because of the increase of source to film distance and biological shield weight is increased because of the increased source to crystal distance.

The higher energy lines are those with lowest overall efficiency, therefore it is very important that all of the source width be effective on the high energy side. In some cases a partially effective source width for the lower energy lines is acceptable because of the higher instrument efficiency.

It is also true that lower energy rays for which the

source width is only partially effective could be detected except that they get blocked out by the right hand part of the cross over shield. If this shielding is moved to allow passage of these rays, the high energy limit is lowered because of the direct beam blackening. A direct shield placed as shown in Figure (29) can help this situation by shielding the direct beam and thus maintaining the high energy limit at the same value while the cross over shield lowers the low energy limit. This procedure was found valuable in allowing some x-rays to be detected in the same exposure as higher energy lines.

Prior to exposure of an emulsion to a source, the authors determined the energy range of greatest interest. Various source positions were then checked for energy limits by using a string technique. The source exposure container was placed in a position estimated from past experience. A string was then stretched from the left edge of a dummy source in the exposure container to the left edge of the crystal, then straight to point A of Figure (29), where A is the virtual image of A'. This determines the low energy cut-off. An energy scale was extended to the virtual image side of the focal circle so that the low energy cut-off could be read directly at A. Similarly, using the right edge of the dummy source and right or high energy side of the crystal, the high energy cut-off could be read at B.

The portion of film blackened by the direct beam was then checked by stretching the string from the left edge of the source to the right edge of the crystal, which was made

coincident with the direct shield, and then straight to point C. The energy of point C was read from the energy scale on top of the film holder. The energy read directly at point C was decreased to allow for scattering and diffraction of the direct beam and secondary radiations. A linear dimension allowance of 1/4" was found sufficient. Since the energy scale is not linear, the amount subtracted from the energy value of C depends on the energy value itself. Clearance through the cross over shield was also checked using strings to simulate rays.

The string technique discussed here proved amazingly sound for predicting the energy range over which an emulsion could be relied upon to receive rays from a given source position. As a practical matter, all emulsions exposed in these experiments were from one of three source positions. The reference lines from the tantalum source were from a position which passed energies of 50 to 175 Kev, with direct darkening at 500 Kev. A higher energy position of 75 to 400 Kev, with direct darkening at 500 Kev was used for some exposures. A third position passing energies of 55 to 250 Kev, with direct blackening at 290 Kev was used for samarium.

It was discovered in the conduct of these experiments that reasonably exact source positions are required. Also of importance is the ability to reposition a source once it has been removed in the middle of a film exposure for reirradiation in the reactor. The source exposure container described in Section III C (3) was adequate in maintaining a position once established and in allowing removal and accurate repositioning. This container has the considerable advantage of being light enough

so that one person can move it or adjust its position. Biologically it is not adequate. Figure (30) shows a source being inserted into the exposure container.

2. Source shielding

Only very approximate source shielding calculations were made. The same general assumptions were used as in Section III C (2). It was found that a four inch lead wall around the exposure container would provide adequate personnel shielding for all sources used in this thesis. The lead wall was built with standard lead bricks. The weight of the shield was about 1000 lbs, which was acceptable from the standpoint of floor and table loadings.

Figure 30 - Method of source insertion into source exposure container. Funnel and guide block are replaced by lead top after source is in the container.

D. SOURCE IRRADIATION AND HANDLING PROCEDURES

It has been mentioned previously that the Cauchois geometry spectrograph, with its extended source, permits the use of relative intense sources of gamma rays. The M.I.T. research reactor was used to irradiate samples of rare earth oxides to prepare these sources. It is the purpose of this section to describe the calculations and procedures involved in the preparation, irradiation, and handling of these sources.

Before making any calculations, it was necessary to estimate the integrated activity to which it was desired to expose each plate. For example, it was experimentally determined that about 55 curie-hours of Ta^{182} exposure were adequate to give strong calibration lines on each plate. The branching ratios of the rare earth isotopes investigated are in general not known with sufficient accuracy to permit precise determination of integrated activity for a specified gamma ray line. Since the present investigations were largely exploratory, it was desired to obtain as many gamma lines from the rare earth isotopes as possible in the time available. To this end, it was found convenient to attempt to get about 50 curie-hours exposure on each of the rare earth plates. Where feasible, longer exposures are obviously desirable to permit some of the less intense gamma ray lines to appear.

Once the goal of 50 curie-hours has been established, it was possible to calculate the source strengths required for various lengths of exposure time. Obviously, the stronger the source, the shorter the time required in the spectrograph. However, there are three practical limits imposed on source

strengths. First, the activation rates in the reactor were generally low, requiring irradiations of several days to a week. This is a result of the fact that the major portion of the neutron captures produce stable isotopes. The short time available for this portion of the thesis did not permit extended irradiations. The second limitation of source strength was the saturation activity reached in the reactor for the short half-life isotopes. In these cases, repeated irradiations and film exposures were required to achieve 50 curie-hours. The third limitation was the consideration of the adequacy of the shielding in the handling equipment, and the estimated dose rate which would be received in handling the source. The last limitation was found to be far less restrictive than the first two. Actual irradiation times, source strengths, and film exposure times were determined for each rare earth sample as a compromise of the above considerations.

Once the desired source strength had been determined, preliminary calculations of reactor irradiation time were made. For this purpose, the samples were assumed to contain 20 gms of the rare earth powder, and the surface area of the active material, which is of interest in black body calculations, was taken as 30 cm^2.

The majority of the rare earth samples have neutron absoption cross sections of the order of thousands of barns. Therefore, many of the samples were effectively "black bodies" or "gray bodies" to the neutron flux. Estimates of the flux depression in the sample were made, using methods similar to

diffusion control rod theory. However, these methods offered little gain in accuracy over engineering estimates based on past experience, i.e. the additional calculation time is not worth the effort. The container walls were found to have little effect on the flux.

Once the preliminary calculations had been refined and checked, a trial irradiation was conducted for each sample. This irradiation time was usually of the order of 1/10 that calculated to be required for full source strength. Following the trial irradiation, the actual source strength produced was measured by a "Juno" survey meter in a fixed geometry arrangement. In this geometry, the source could be accurately positioned at one meter from the measuring device. The source strength was then calculated from the relation

$$C = \frac{R \times d^2}{5.20 \times 10^6 \times E}$$

where C = source strength in curies

R = measured dose rate in mr/hr

d = distance, source to detector in cm

E = average energy of electromagnetic radiation emitted by source

Although this relation is approximate at best, and is subject to inaccuracies, it provided results adequate for the present purpose.

The measured source strength permitted refined calculations to be made for activation rates and irradiation

times in the reactor. The prime uncertainty that the test irradiation resolved was the admittedly gross estimate of the flux depression in the sample.

The sample was inserted in the vertical facilities 3GV5 or 3GV6 of the reactor, using a gripping device which attached to the top hat of the sample container. The sample container is shown in Figure 17. Before insertion in the reactor, the entire sample surface was carefully cleaned with acetone to remove any possible foreign material which could be activated by the neutron flux. However, on removal from the reactor, the samples were usually found to carry varying degrees of surface contamination. Surface wipes, made with acetone soaked paper tissues, were conducted behind lead shields. Four surface wipes were usually sufficient to reduce the contamination received on a dry wipe test to about .5 mr/hr. Fortunately, all the contamination observed decayed with a half - life of two to three hours, and so did not constitute a long term hazard.

Following a satisfactory wipe test, the radioactive sample was transferred to one of the shielded transportation containers described in Part C, Section III, for movement to the spectrograph area. On arrival in Room 320, the source strength was measured with the "Juno" meter in the fixed geometry. After this, the source was placed in the exposure container, as shown in Figure 30, and the exposure started.

Handling of the source from the lead shielded transportation container, to the fixed geometry, to the exposure container (and from the exposure container to the storage vault after completion of the exposure) is accomplished by one meter long tongs.

This is the only time during the entire handling procedure that personnel were necessarily exposed to an unshielded source. It is during this period that the highest dose rates were received. With practice, it was found that the person handling the source need be directly exposed only about 10 seconds. Because of the high energy gamma rays emitted, the most difficult isotope to handle was the 1.8 curie Ta^{182} calibration source. Average doses received in its handling were from 3 to 5 mr. It is emphasized, however, that considerable care is required at all times when handling sources of this magnitude.

Table I is a summary of all rare earth source irradiations and film exposures made during the conduct of this thesis.

TABLE I

Radioactive Source Summary

Isotope	Half-Life	Source strength at start of exposure (curies)	Film integrated activity (curie-hours)	Lines Measured (Kev)	Remarks
Nd^{147}	11.3 days	.27	18.2	91	
Sm^{153}	47. hrs.	.71 to 1.6	94.0	70, 97, .103	Total of 4 different irradiations exposures
Dy^{165}	2.32 hrs.	21.6	71.6	95	
Er^{171}	7.5 hrs.	1.6 to 2.0	45.8	112, 124, 308	Total of 3 different irradiations α exposures
Yb^{169}	32. days	1.90	164.	110,131,177,198	First Yb plate
Yb^{175}	4.1 days	3.16	211.	114,145,282,396	
Yb^{169}	32. days	.94	51.6	64, 110	Second Yb plate
Yb^{175}	4.1 days	.36	19.7	114	

Note: Integrated radioactivity in curie-hours applies to best estimates of total source activity, not to transitions by any particular gamma ray branch.

E. DETECTION PROCEDURES

Detector requirements for measurement of gamma ray energies with high precision using a bent crystal spectrograph are:

(1) Detector resolution at least equal to the crystal resolution

(2) Highest possible efficiency for detecting gamma and x-rays of all energies

(3) If a counter is used, the detector must be stable because data collecting periods will be long due to low intensity of diffracted rays.

(4) Reliable as possible

It is apparent from these requirements that an ideal detector is almost impossible to attain. The best detector developed to date for the Cauchois geometry instrument is Ilford G-5, 600 micron thick emulsion, mounted on thin glass plates. Such emulsions were used in these experiments. This detection system allows simultaneous detection of gamma and x-rays over wide energy bands.

These emulsions require special care. They must be protected from light and extraneous electromagnetic radiations at all times. Storage in a moist atmosphere is required to prevent the emulsion from drying out. Double thickness light tight envelopes were made from heavy black construction paper. To prevent the emulsion from sticking to the light tight envelopes, it was necessary to wrap the glass backed emulsion plates in thin plastic such as "Saran Wrap" prior to insertion into the envelopes. To avoid high background radiations, the emulsions were stored in a darkroom, far removed from the experimental area. The storage

atmosphere was kept moist by the evaporation of water from a pan in the drawer.

Precision measurement of gamma ray energies depends on accurately measuring the distance between lines on the emulsion. Therefore, it is vital that shrinkage of the emulsion be minimized. Placing the emulsion on glass to which it adheres tightly has proved a satisfactory method of minimizing the shrinkage. However, introduction of glass into the detection system reduces the reliability. The mounting must be flexible enough so that the emulsion can be bent in the film holder to conform to the focal circle. The authors found the glass thickness to be quite critical. Two out of three plates of .033 inch thickness cracked during exposure, while none of the seven plates of .027 inch thickness cracked during this period. One of the thinner plates did crack, however, during shipment or developing. The thicker plates apparently did not crack while being inserted and bent in the film holder. The glass cracked sometime later, while still bent to the one meter radius of the focal circle. The thicker glass could quite probably be used in a spectrograph of larger radius.

Estimates of exposure times required to produce readable lines were based on measured source strengths and published branching ratios (23), where known. At 100 kev, an exposure of one curie hour has been found sufficient by the authors of reference (8). Since the efficiency of the instrument decreases by a factor of 100 at 300 kev, considerably longer exposure times are required for the higher energy gamma lines. In practice very few of the branching ratios of the isotopes in the

region of investigation are known with sufficient accuracy to permit accurate estimates of exposure time. As a goal, all rare earth elements were exposed for approximately 50 curie hours. Wherever possible, and as time permitted, longer exposures were made. For example, the dysprosium source was exposed for approximately 72 curie-hours and the ytterbium source for 164 curie-hours of Yb^{169} and 211 curie-hours of Yb^{175}.

For reference lines, the K x-rays from Ta and W, and the 68 kev and 100 kev nuclear lines in W were placed on each plate with a Ta^{182} source. It was found that detectable lines could be obtained with about 35 curie-hours, but lines of much better readability resulted from 55 curie-hours.

Rough checks of emulsion exposure time were obtained by placing two separately packaged x-ray films in front of the emulsion. These films were taped onto the front of the film holder, and so could be removed for development without disturbing the emulsion. The lines recorded on the x-ray film were not in good focus, being almost 1 1/2 inch inside the focal circle. However, the intense x-ray lines from the source were readily detected on the film and some low energy gamma rays were intense enough to also be detected. These films were developed while the emulsion was still in the film holder. A decision, based on the film results, was made on whether to terminate or continue the exposure of the emulsion. These films and their light tight envelopes also perform the function of stopping soft secondary radiations from reaching the emulsion. This lessens the general darkening of the emulsion.

SECTION V - DATA REDUCTION AND CALCULATIONAL METHODS

A. MEASUREMENT OF LINE POSITIONS

The operation of the bent crystal spectrograph depends on the fact that the position of a gamma ray line along the focal circle is a measure of its energy. The precision of the present method of energy determination is made possible by the capability of making highly accurate measurements of relative linear positions of gamma ray lines recorded on a nuclear emulsion along the focal circle.

Besides the gamma lines from the rare earth source, each plate contains the K_α and K_β x-rays and two nuclear lines from the Ta^{182} calibration source. In most cases, five calibration lines were measured, Ta K_{α_1}, W K_{α_1} and K_{α_2} and the 68 kev and 100 kev gamma lines from tungsten.

Measurements of the line positions were made on an optical comparator available in the Spectroscopy Laboratory at M.I.T. The comparator was manufactured by Adam Hilger, Ltd., London, and has scale graduations, including Vernier, for distances to .001 mm. To provide statistically significant data for the calculations, each of the five calibration lines and each of the unknown gamma lines were read by at least three separate observers. Each observer would read the plate from left to right three times in succession, taking care to work all backlash from the screw drive after each reversal of direction of motion. The entire procedure was then repeated by all observers, after having turned the plate end for end. Again the reading was from left to right on the comparator, but in this case, the plate was traversed in the opposite direction. This procedure was adopted in order to avoid systematic errors from

possible imperfections in the screw drive.

The left and right edges of each line are measured, and then averaged to obtain the position of the line center. Center line positions, reproducible to within about .020 mm were obtained in this manner. As an added precaution to eliminate systematic errors, the plates were shifted vertically between each pass to place the field of vision of the microscope on a different part of the plate.

B. CALCULATION OF GAMMA RAY ENERGIES

In principle, Bragg's Law determines the wavelengths of the lines observed on the emulsion. We may state Bragg's Law in an applicable form as:

$$\frac{\lambda}{2d} = \sin\left(\frac{h-h_o}{R}\right)$$

where λ is the wavelength of the line

d is the grating constant of the (310) planes of quartz used for the reflection

$(h-h_o)$ is the line position measured from the β point along the focal circle

R is the diameter of the focal circle

The wavelengths expressed in x units (Seigbahn scale) may be converted into energies, E, in kev by using the conversion constant given by DuMond and Cohen in reference (6) as

$$E = \frac{12372.44 \pm 0.16}{\lambda}$$

The quantity 2d for the (310) planes of quartz has been determined by a number of observers and is reported in reference (21). We have used the value at 20°C, $2d = 2355.34 \pm 0.04$ x.u., from reference (21).

It can be seen from the Bragg Law that any pair of calibration lines, with their known wave lengths will yield a set of two simultaneous equations in the unknowns R and h_o. Actually R is an instrument constant, which can in principle be measured. It has been found, however, that direct measurements of R result in less precise values than the R determined from the calibration lines. By solving for R and h_o from a known

pair of calibration lines, and introducing h_3, the measured position of the unknown line, the unknown wave length may be determined. The resulting expression, from reference (7) is obtained, keeping only the first two terms of the power series expansion for the arcsin:

$$\lambda_3 = \lambda_2 + \frac{h_3 - h_2}{h_1 - h_2}(\lambda_1 - \lambda_2)\left[1 - \frac{1}{6}\left(\frac{\lambda_3 - \lambda_1}{2d}\right)\left(\frac{\lambda_1 + \lambda_2 + \lambda_3}{2d}\right)\right]$$

where λ_1 and λ_2 are the wave lengths of the calibration lines, and h_1 and h_2 their measured positions. The correction term is of the order of 0.1% and need not be evaluated with great precision.

There will, in general, be available more than the two calibration lines necessary to solve for λ_3. Therefore, there will be several values of λ_3 obtained. A rigorous method of finding the mean or best value is practical only if the calibration line data is statistically independent. If all possible calibration pairs are formed from the lines measured, i.e. three pairs from three calibration lines, it is clear that the values so obtained are not statistically independent. From consultation with Prof. Hans Mark, one of the authors of references (7) and (9), it was determined that the method of calculation of the Livermore group had been modified for this reason. The calculational methods of reference (9) are therefore used as a guide in this thesis.

The method of calculation used here is essentially that of reference (9) up to the completion of the least squares solution for R and h_o. It is convenient to state Bragg's Law as follows:

$$\arcsin \frac{\lambda}{2d} = \frac{h - h_o}{R}$$

We have used five calibration lines on each plate. Wave length values for these reference lines are given in Appendix B. Any pair of calibration lines will determine values of h_o and R. Five calibration lines will overdetermine R and h_o, therefore a least squares solution was used to find the "best" values of R and h_o. The least squares solution was obtained by fitting the calibration line data to a relation of the form

$$Rx + h_o = h$$

where $x = \arcsin \frac{\lambda'}{2d}$ with λ' = wavelength of a calibration line

The specific formulas used for calculating R and h_o are taken from reference (26) as follows:

$$R = \frac{n\sum_{i=1}^{n} h_i X_i - \sum_{i=1}^{n} X_i \sum_{i=1}^{n} h_i}{n\sum_{i=1}^{n} X_i^2 - \left(\sum_{i=1}^{n} X_i\right)^2} \qquad (1)$$

$$h_o = \frac{\sum_{i=1}^{n} X_i^2 \sum_{i=1}^{n} h_i - \sum_{i=1}^{n} X_i \sum h_i X_i}{n\sum_{i=1}^{n} X_i^2 - \left(\sum_{i=1}^{n} X_i\right)^2} \qquad (2)$$

where n is the number of calibration lines

Each set of observations made by one observer in a single traverse of the plate yields statistically independent data. A least squares determination of R and h_o was therefore made

for each such set of data.

The wavelengths of the unknown lines were then computed by using the observed values of h with the least squares values of R and h_o from the same set of observations. Hence, each unknown wavelength was calculated for each observer for each traverse across the plate. Usually eighteen such observations were made for each plate. The resulting eighteen values of λ are statistically independent, avoiding the difficulty of averaging statistically dependent quantities that was encountered in the previous method. Each value of λ has the same weight, therefore

$$\overline{\lambda} = \frac{\sum_{i=1}^{n} \lambda_i}{n}$$

Sample calculations are shown in Appendix A for the 95 kev line of Ho^{165}. All values of wavelength reported in this thesis were calculated by hand using a desk calculator. The data from the various observers was inspected in an attempt to discover systematic errors. None were observed.

C. DETERMINATION OF STANDARD DEVIATION

We again start with Bragg's Law in the form:

$$\lambda_i = 2d \quad \arcsin \frac{hi - he}{R}$$

where nomenclature is the same as in Section V, Part B. Next, we make the approximation that $\arcsin\left(\frac{hi - he}{R}\right) \simeq \left(\frac{hi - he}{R}\right)$, i.e. the angles are small. The reader may easily convince himself that this is an excellent approximation for the purpose of propagating errors. The rules for the propagation of errors for differences and for products and quotients have been used to derive the following expression for the standard deviation of the calculated wave length:

$$\sigma(\lambda_i) = \sqrt{\lambda_i^2 \left[\left(\frac{\sigma_d}{d}\right)^2 + \left(\frac{\sigma_{hi}^2 + \sigma_{he}^2}{(hi - he)^2}\right) + \left(\frac{\sigma_R}{R}\right)^2 \right]} \qquad \text{Eq. (4)}$$

From reference (21), we can calculate $\left(\frac{\sigma_d}{d}\right)^2$ as 3×10^{-10}. After evaluation of the other terms, we will find that the contribution of $\frac{\sigma_d}{d}$ is negligible.

The evaluation of σ_R and σ_{h_e} is not straight forward from the least squares solution described in Part B because the assumption was made there that no error existed in the values of the calibration wave lengths. This assumption was made in order to get a least squares calculation that is amenable to hand methods. It does not significantly affect the final values reported for the measured wave lengths. However, a standard deviation calculation based on this assumption would ignore the deviations in the calibration wave lengths that are known to exist, and therefore would predict too small an error for R and h_e.

Rigorously speaking the calculation of σ_R and σ_{h_e} should

come from a determination of the correlation coefficient between R and $h_\bullet$. This is a long and cumbersome process for hand calculations yielding values of $\sigma(\lambda_i)$ not much different than the ones reported here. The $\sigma(\lambda_i)'s$ reported in this thesis were calculated by an approximate method to be described. We feel that the approximate calculations for $\sigma(\lambda_i)$ are valid because values obtained compare favorably with the values reported in reference (9), which were machine calculated by the rigorous method.

A good estimate of the standard deviation of the reported wave length values may be obtained by the following approximate analysis of error propagation. We know from physical reasoning, and it can also be verified from the least squares formulas, that R and $h_\bullet$ are functions of h_i' and λ_i', where h_i' is the position and λ_i' the wave length of the calibration lines. A primed quantity refers to the calibration lines. This information plus the general law for propagation of errors enables us to get valid approximate values of R and $h_\bullet$. From the general law for propagation of errors, we get

$$(\sigma_R)^2 = \sum_{i=1}^{n} (\sigma_{i'})^2 \left(\frac{\partial R}{\partial \lambda_i'}\right)^2 + \sum_{i=1}^{n} (\sigma_{h_i})^2 \left(\frac{\partial R}{\partial h_i'}\right)^2 \qquad \text{Eq. (5)}$$

and

$$(\sigma_{h_\bullet})^2 = \sum_{i=1}^{n} (\sigma_{\lambda_i})^2 \left(\frac{\partial h_\bullet}{\partial \lambda_i'}\right)^2 + \sum_{i=1}^{n} (\sigma_{h_i'})^2 \left(\frac{\partial h_\bullet}{\partial h_i}\right)^2 \qquad \text{Eq. (6)}$$

We must now evaluate each of the derivatives and also determine $\sigma_{i'}$ and $\sigma_{h_i'}$. From the first order approximation of Bragg's Law, $R \approx \frac{2d}{\lambda_i'} \left[h_i' - h_\bullet\right]$

and hence $\frac{\partial R}{\partial \lambda_i'} \cong -\frac{R}{\lambda_i'}$ $\frac{\partial R}{\partial h_i'} \cong \frac{R}{h_i' - h_o}$

For each plate, we calculate a mean value of R from the 18 least squares values available. Similarly we obtain a mean value for h_o. The values of λ_i' are known and the values of $(h_1' - h_o)$ are calculated from the observed h_1' and the mean h_o for the plate.

We assume that $\sigma_{\lambda_i'}$ is the same for all calibration wave lengths. The value of $\sigma_{\lambda_i'}$ used here is .02 x.u. This is the largest of all the $\sigma_{\lambda_i'}$ of the calibration wave lengths used in these experiments. This assumption simplifies the calculations considerably and introduces very little error into the calculations of σ_R. Any error so introduced is on the conservative side.

By inspection of the data, we chose a reasonable value for $\sigma_{h_i'}$ as 0.01 mm. We also assume that all measurements have the same deviation. This assumption further simplifies the calculations and any error introduced is on the conservative side.

We now have numerical values for each term needed to calculate σ_R. The value of σ_R calculated from data obtained from the dysprosium plate was .40 mm. Using completely analogous approximations for $\frac{\partial h_o}{\partial \lambda_i'}$, and $\frac{\partial h_o}{\partial h_i'}$, and the same value for $\sigma_{h_i'}$ and $\sigma_{\lambda_i'}$, we found $\sigma_{h_o} \cong .03$ mm.

In order to further check the validity of these approximations, we calculated the partial derivatives

$$\frac{\partial R}{\partial \lambda_i'}, \quad \frac{\partial R}{\partial h_i'}, \quad \frac{\partial h_o}{\partial \lambda_i'} \quad \text{and} \quad \frac{\partial h_o}{\partial h_i'}$$

by differentiating the least squares formulas for R and h_o, equations (1) and (2) and then evaluating the resulting equations for the dysprosium data. The differentiation resulted in the following equations:

$$\frac{\partial R}{\partial \lambda_i'} = \frac{D\left\{nh_i - \sum_{i=1}^{n} h_i\right\} - N\left\{2n X_i - 2\sum_{i=1}^{n} X_i\right\}}{2d\ D^2}$$

where D = denominator of equation (1)

N = numerator of equation (1)

n = number of calibration lines

$$\frac{\partial R}{\partial h_i} = \frac{nX_i - \sum_{i=1}^{n} X_i}{D}$$

$$\frac{\partial h_o}{\partial \lambda_i} = \frac{D\left\{2X_i \sum_{i=1}^{n} h_i - \sum_{i=1}^{n} h_i X_i - h_i \sum_{i=1}^{n} X_i\right\} - N'\left\{2nX_i - 2\sum_{i=1}^{n} X_i\right\}}{2d\ D^2}$$

where N' = numerator of equation (2)

$$\frac{\partial h_o}{\partial h_i} = \frac{\sum_{i=1}^{n} X_i^2 - X_i \sum_{i=1}^{n} X_i}{D}$$

As an example of the agreement between the approximate method and the above formulas from least squares, the following values for $\frac{\partial R}{\partial \lambda_i'}$ are given:

	Least Squares Differentiation	Approximate Relation
$\frac{\partial R}{\partial \lambda_1'}$	12.15	9.30
$\frac{\partial R}{\partial \lambda_2'}$	10.28	9.52
$\frac{\partial R}{\partial \lambda_3'}$	10.7	10.87

Other derivatives were similarly evaluated with the same degree of agreement with the approximate method.

By inspection of the calculated values for R_o and $(h_i' - h_o)$, we found that R and $(h_i - h_o)$ were nearly the same for all plates.

With these generalizations and with the above approximations shown to be reasonable, it follows that $(\frac{\sigma_R}{R})^2$ and $(\sigma_{h_o})^2$ need be calculated only once for a given set of calibration lines used with a given spectrograph. We have used $(\frac{\sigma_R}{R})^2 = 4 \times 10^{-8}$ and $(\sigma_{h_o})^2 = 9 \times 10^{-4}$ mm^2. Therefore, $(\sigma_{h_i})^2 + (\sigma_{h_o})^2 = 10 \times 10^{-4}$ mm^2. These values introduced into equation (4) give

$$\sigma(\lambda_i) = \sqrt{\lambda_i^2 \left[\frac{10 \times 10^{-4}}{(h_i - h_o)^2} + 4 \times 10^{-8} \right]} \qquad \text{Eq. (7)}$$

where $(h_i - h_o)$ is in mm.

Finally, the conversion of $\sigma(\lambda_i)$ to $\sigma(E_i)$ may be made by keeping the fractional deviations equal, i.e. $\frac{\sigma(\lambda_i)}{\lambda_i} = \frac{\sigma(E_i)}{E_i}$. This is true because the fractional deviation of the conversion constant is so small.

SECTION VI - RESULTS

Table II contains the wave lengths and energies of all gamma rays measured during the conduct of this thesis. A total of seventeen different gamma rays, emitted from five different odd Z isotopes, from Z = 61 to Z = 71, were measured.

Of the seventeen energies included, fifteen have been previously measured by crystal spectrometer methods, either in the Mark I geometry at Cal. Tech. (references g and h of Table II) or Sweden (a, b), or in the Cauchois geometry at Livermore (c). Agreement with these earlier precision measurements is considered quite satisfactory.

Two of the energies determined, those of the 91 kev line in Pm^{147} and the 97 kev line in Eu^{153}, have been determined here by the precise crystal method for the first time. The previous determinations of these energies has been by scintillation counter or beta spectrometer methods. The present method improves the accuracy to which these values are known by one order of magnitude.

The 97 kev line of Eu^{153} deserves special comment in that this particular gamma ray has been reported by only one group of investigators, Church and Goldhaber in reference d of Table II. There it is reported that the decay of Gd^{153} yields transitions of 69.4, 97.3 and 103.1 kev in Eu^{153}. Only the first and last of these are reported to have been seen following the decay of Sm^{153}. The 97 kev line was obtained in the present case from the decay of Sm^{153}. It is also noted that other articles, references a, b, e, f, and j of Table II, which report observed gamma transitions characteristic of the decay of Sm^{153} have failed to observe this 97 kev gamma ray.

TABLE II

Measured Wavelengths and Energies of Gamma Rays

Parent Isotope	Daughter Product (Gamma Emittor)	Wavelengths in Siegbahn X units	Energy in Kev	Best previous values of energy	Reference
Nd^{147}	Pm^{147}	135.88 ± .05	91.05 ± .04	91.3	e*
Sm^{153}	Eu^{153}	177.60 ± .05	69.66 ± .02	69.66	b
		127.00 ± .05	97.42 ± .04	97.3	d*
		119.92 ± .05	103.17 ± .04	103.27 ± .02	a
Dy^{165}	Ho^{165}	130.75 ± .05	94.63 ± .04	94.793 ± .007 94.70 ± .02	a c
Er^{171}	Tm^{171}	110.86 ± .04	111.61 ± .04	111.63 ± .02	h
		99.79 ± .04	123.98 ± .06	124.03 ± .03	h
		40.34 ± .04	306.70 ± .30	308.37 ± .15	h
Yb^{169}	Tm^{169}	196.05 ± .05	63.11 ± .02	63.12 ± .01	g
		112.72 ± .04	109.77 ± .04	109.78 ± .02 109.77 ± .03	g c
		94.79 ± .04	130.53 ± .06	130.53 ± .03	g

* Values not previously measured by crystal spectrometer

TABLE II (cont.)

Parent Isotope	Daughter Product (Gamma Emittor)	Wavelengths in Siegbahn X units	Energy in Kev	Best previous values of energy	Reference
Yb^{169}	Tm^{169}	69.79 ± .04	177.27 ± .10	177.24 ± .05	g
		62.49 ± .04	197.99 ± .13	197.97 ± .06	g
Yb^{175}	Lu^{175}	108.74 ± .04	113.78 ± .04	113.81 ± .02 113.79 ± .04	g c
		85.40 ± .04	144.88 ± .07	144.85 ± .03	g
		43.83 ± .04	282.30 ± .26	282.57 ± .13	g
		31.31 ± .04	395.1 ± .4	396.1 ± .3	g

REFERENCES FOR TABLE II - RESULTS

a) B, Anderssen, Proc. Phys. Soc. (London) 69A, 415 (1956)

b) O. Beckman (to be published), quoted in D. Stromínger, J. M. Hollander and G. T. Seaberg, Rev. Mod. Phy. 30, 585 (1958)

c) E. L. Chupp, J. W. M. DuMond, F. J. Gordon, R. C. Jopson and Hans Mark, Phys. Rev. 112, 518 (1958)

d) E. L. Church and M. Goldhaber, Phys. Rev. 95, 626A (1954)

e) J. M. Cork, M. K. Brice, R. G. Helmer and R. M. Woods, Jr., Bull. Am. Phys. Soc. Ser. II, 3, 64 (1958)

f) R. L. Graham and J. Walker, Phys. Rev. 94, 794A (1954)

g) E. N. Hatch, F. Boehm, P. Marmier and J. W. M. DuMond, Phys. Rev. 104, 745 (1956)

h) E. N. Harch and F. Boehm, Phys. Rev. 108, 113 (1957)

i) Phys. Rev. 92, 1271 (1953)

j) N. Marty, J. phy. et radium 16, 458 (1955)

SECTION VII - CONCLUSIONS AND RECOMMENDATIONS

A. CONCLUSIONS

The initial objective of the thesis has been accomplished. The two meter spectrograph has been aligned, calibrated and placed in operation. Satisfactory techniques have been developed for the preparation, irradiation, handling and storage of the several curie sources used with the spectrograph. Gamma ray energies calculated from the measured displacement of the spectra along the focal circle show satisfactory agreement with earlier crystal spectrometer values. This is believed to be adequate confirmation of the successful operation of the spectrograph. Two gamma ray energies have been measured for the first time to the precision made possible by the bent crystal spectrograph.

B. RECOMMENDATIONS

Recommendations for the continuation of the experimental work and refinements of techniques may be summarized as follows:

(1) Develop a program for the M.I.T. Computational Center IBM 704 Digital Computer. This program should be based on a least squares determination of R and h_o where the data is fitted to the form $Rx + h_o = y$, where errors are permitted in both x and y. The end result of the machine calculations should be the wavelength of the line and its standard deviation, both calculated by rigorous statistical methods.

(2) Continue the irradiation of samples and their exposure in order to extend the range of gamma rays that have been measured by this precision method. Special attention should be given to isotopes not previously analyzed by crystal spectrometers.

(3) Further extend the measurement of gamma rays, especially into the region of short half-life isotopes, by setting up the spectrograph on the reactor floor and exposing sources which are being irradiated in one of the through-ports in the reactor.

(4) Make relative intensity measurements of gamma rays by placing a scintillation crystal behind a narrow slit arrangement along the focal circle. The slit arrangement would be used to shield the crystal from all except one gamma ray line. The crystal would provide the high degree of energy resolution so desirable for these measurements. Such a series of data would provide additional information on branching ratios and decay schemes of the isotopes measured.

(5) Design and manufacture a new crystal holder mounting block which provides positive locking devices for the crystal holder. This can be done by using tapered machined pins which position the crystal holder in the mounting block as well as securely fastening it. This recommendation is based on the authors' experience of having the crystal holder move relative to the mounting block during one of the Hartmann tests. During the rest of these experiments, extreme care was used to prevent a recurrence.

(6) The film holder base should be made lighter and a better method of securing it to the frame should be devised. This could be accomplished by drilling holes in the base which are judiciously placed so that they match up with the tapped holes in the frame for a variety of film holder positions.

APPENDIX A

Sample Calculations:

In this appendix the calculations for the dyspresium plate will be given as a sample of the routine calculational procedures performed for each plate. The dyspresium plate was picked for use as a sample because these calculations were completed first. They are also shorter than most because only one unknown line appeared on this plate.

The following table of data for the reference lines was computed from the λ_is of the reference lines, the value of 2d, and the series expansion of the arcsin $\frac{\lambda i}{2d}$. The first three terms of the series, arcsin $X = X + \frac{X^3}{2.3} + \frac{1.3\ X^5}{2.4.5} + \ldots$, were used. This was sufficient to calculate the value of the arcsin $\frac{\lambda i}{2d}$ accurate to six significant figures.

TABLE III

Plate D Date 7/4/59

i	Reference Lines	λ_i in X. U.	i/2d	X_i = ARCSIN $\frac{\lambda i}{2d}$	X_i^2
1	$T_A - K\alpha_1$				
2	$W - K\alpha_2$	213.382	.090595	.0907194	.0082300
3	$W - K\alpha_1$	208.571	.088552	.0886685	.0078621
4	$T_A - 68$	182.638	.077542	.0776200	.0060249
5	$T_A - 100$	123.599	.052476	.0525002	.0027563
			$\sum X_i =$	.3095081	$\sum X_i^2 =$ .0248733
			$(\sum X_i)^2 =$	.0957953	$n\sum X_i^2 =$ .0994932

We used the following formulas to determine the least square "best" values for R and h_o : (See Section V, B)

$$R = \frac{n \sum_{i=1}^{n} X_i Y_i - \sum_{i=1}^{n} Y_i \sum_{i=1}^{n} X_i}{n \sum_{i=1}^{n} X_i^2 - \left(\sum_{i=1}^{n} X_i\right)^2}$$

$$h_o = \frac{\sum_{i=1}^{n} Y_i \sum_{i=1}^{n} X_i^2 - \sum_{i=1}^{n} X_i \sum_{i=1}^{n} X_i Y_i}{n \sum_{i=1}^{n} X_i^2 - \left(\sum X_i\right)^2}$$

Combination of the appropriate values from Table III gives a value of .0036979 for the common denominator of both equations.

Y_i is the value, in millimeters, of the center of the line. Y_i is obtained as the average of the left and right edge comparator readings of a single observer during one traverse of the plate.

These calculations for R and h_o were done in tabular form with the indicated operations performed by desk calculator. The completed forms are Tables (IV) and (V).

Next, $(h - h_o)$ for the unknown line was calculated for each pass for each observer. These were done on a desk calculator using the values of h_o from Table (V) and the values of h from the raw data sheets. The results were recorded in tabular form in Table (VI). As before, the values of Table VI were computed using a desk calculator except that slide rule accuracy is sufficient for the quantity $\frac{1}{6}\left(\frac{h - h_o}{R}\right)^3$.

The value of λm = 130.746 X. U. is converted to energy by $E = \frac{12,372.44}{130.746}$ = 94.63 kev.

We found the standard deviation from Eq. (7):

$$\sigma(\lambda) = \sqrt{(130.746)^2 \left[\frac{10 \times 10^{-4}}{(110.2)^2} + 4 \times 10^{-8} \right]} = \pm .05 \text{ x.u.}$$

$$\frac{\sigma(\lambda)}{\lambda} = \frac{.05}{130.746} = \frac{\sigma(E)}{E}$$

$$(E) = \frac{.05(94.63)}{130.746} = \pm .036 = \pm .04 \text{ kev.}$$

Find values for $H_{\bullet}^{165}$ gamma ray at 94.63 $\pm$ .04 kev.

TABLE IV

Plate D Date: 7/4/59

Reading No.	1	2	3	4	5	6	7	8	9
Y_1									
Y_2	28.143	28.142	28.153	27.860	27.897	27.880	96.560	96.552	96.584
Y_3	32.197	32.189	32.184	31.962	31.964	31.961	92.490	92.450	92.503
Y_4	54.189	54.174	54.184	53.934	53.972	53.950	70.496	70.474	70.512
Y_5	103.998	103.968	104.013	103.816	103.776	103.811	20.686	20.651	20.687
$\sum Y_i$	218.527	218.473	218.534	217.572	217.609	217.602	280.232	280.127	280.286
$\sum X_i \sum Y_i$	67.6356	67.6189	67.6378	67.3401	67.3515	67.3493	86.7338	86 .7013	86.7505
$\sum X_i^2 \sum Y_i$	5.43542	5.43408	5.43560	5.41167	5.41259	5.41241	6.97021	6.96760	6.97155

Reading No.	10	11	12	13	14	15	16	17	18
Y_1									
Y_2	99.806	99.858	99.852	94.314	92.256	89.098	24.092	22.894	21.677
Y_3	95.709	95.714	95.718	90.258	88.176	85.028	28.214	26.987	25.767
Y_4	73.764	73.764	73.760	68.272	66.200	63.064	50.189	48 .934	47.746
Y_5	23.888	23.932	23.914	18.458	16.374	13.195	100.030	98 .791	97.540
$\sum Y_i$	293.167	293.268	293.244	271.302	263.006	250.385	202.525	197.656	192.730
$\sum X_i \sum Y_i$	90.7372	90.7685	90.7611	83.9699	81.4022	77.4959	62.6829	61 .1759	59.6513
$\sum X_i^2 \sum Y_i$	7.29194	7.29445	7.29386	6.74809	6.54175	6.22783	5.03740	4.91630	4.79377

$\sum X_i = .309507$
$\sum X_i^2 = .024873$
} values from TABLE. III

TABLE V

Plate D — Date: 7/4/59

Reading No.	1	2	3	4	5	6	7	8	9
X_1 Y_1									
X_2 Y_2	2.5 5310	2.55301	2.55401	2.52743	2.53079	2.52925	8.75983	8.75910	8.76200
X_3 Y_3	2.85484	2.85413	2.85369	2.83401	2.83418	2.83392	8.20090	8.19736	8.20206
X_4 Y_4	4.20615	4.20499	4.20576	4.18636	4.18931	4.18760	5.47190	5.47019	5.47314
X_5 Y_5	5.45990	5.45832	5.46068	5.45034	5.44824	5.45008	1.08602	1.08418	1.08607
$\sum X_i\ Y_i$	15.07399	15.07045	15.07414	14.99814	15.00252	15.00085	23.51865	23.51033	23.52327
$n\sum X_i Y_i$	60.29596	60.2818	60.2966	59.9926	60.0101	60.0101	94.0746	94.0433	94.0931
Numerator(R)	-7.3396	-7.3371	-7.3412	-7.3475	-7.3414	-7.3459	+ 7.3408	+7.3420	+ 7.3426
R (mm)	-1984.80	-1984.13	-1985.23	-1986.94	-1985.29	-1986.51	+1985.13	+1985.45	+1985.61
$\sum X_i \sum X_i\ Y_i$	4.66551	4.66441	4.66555	4.64203	4.64338	4.64287	7.27919	7.27677	7.28062
Numerator(ho)	+ 0.76991	+0.7696 7	+ .77005	+ .76964	+.76921	+.76954	− .30898	− .30917	− .3 0907
h_o (mm)	+208.202	+ 208.137	+ 208.240	+ 208.129	+208.013	+208.102	− 83.5555	− 83.6069	−83.5 799

TABLE V (CONTINUED)

Plate D Date: 7/4/59

Reading No.	10	11	12	13	14	15	16	17	18
X_i Y_i									
X_2 Y_2	9.05430	9.05902	9.05847	8.55607	8.36937	8.08288	2.18560	2.07692	1.96652
X_3 Y_3	8.48633	8.48677	8.48712	8.00300	7.81839	7.53926	2. 50168	2.39288	2.28471
X_4 Y_4	5.72556	5.72556	5.72525	5.29927	5.13844	4.89503	3.89567	3.80214	3.70604
X_5 Y_5	1.25412	1.25643	1.25548	0.96904	0.85964	0.69274	5.25158	5.18653	5.12085
$\sum X_i Y_i$	24.52031	24.52778	24.52632	22.82738	22.18584	21.20991	13. 83453	13.45847	13.07812
$\sum X_i Y_i$	98.0812	98.1111	98.1053	91.3095	88.7434	84.8396	55. 3381	53.8339	52.3125
Numerator(R)	+7.3440	+ 7.3426	+ 7.3442	+ 7.3396	+ 7.3412	+ 7.3437	-7. 3448	-7.3420	- -7.3388
R (mm.	+1985.99	+1985.61	+1986.05	+1984.80	+1985.23	+1985.91	-1986.21	-1985.45	-1984.59
$\sum X_i \sum X_i Y_i$	7.58921	7.59152	7.59107	7.06523	6.86667	6.56462	4. 28188	4.16549	4.04777
Numerator (ho)	- .29727	- .29707	- .29707	- .31714	- .32493	- .33679	+ .75552	+ .75081	+ .74600
ho	-80.3839	-80.3348	-80.3726	-85.7622	-87.8688	-91.0760	+204.310	+ 203.037	+201.736

Plate D Date: 7/4/59 Calculation of For Ho 95 Kev

Reading No.	h - ho	$\frac{h - ho}{R}$	$\frac{1}{6}\left(\frac{h - ho}{R}\right)^3$	Sin $\left(\frac{h_a - ho}{R}\right)$	λ in X. U.	λ - m	$(\lambda - m)^2$ X10^{-6}
1	-110.194	+.0555189	.0000285	.0554904	130.699	-.047	2209.
2	-110.127	+.0555039		.0554754	130.663	-.083	6889.
3	-110.260	+.0555402		.0555117	130.749	+.003	9.
4	-110.361	+.0555432		.0555147	130.756	+.010	100.
5	-110.227	+.0555219		.0554934	130.706	-.040	1600.
6	-110.340	+.0555446		.0555161	130.759	+.013	169.
7	+110.262	+.0555440		.0555155	130.758	+.012	144.
8	+110.293	+.0555506		.0555221	130.773	+.027	729.
9	+110.285	+.0555421		.0555136	130.753	+.007	49.
10	+110.333	+.0555557		.0555272	130.785	+.039	1521.
11	+110.303	+.0555512		.0555227	130.775	+.029	841.
12	+110.329	+.0555520		.0555235	130.777	+.031	961.
13	+110.244	+.0555441		.0555156	130.758	+.012	144.
14	+110.266	+.0555432		.0555147	130.756	+.010	100.
15	+110.322	+.0555524		.0555239	130.778	+.032	1024.
16	-110.318	+.0555420		.0555135	130.743	+.007	49.
17	-110.235	+.0555214		.0554929	130.705	-.041	1681.
18	-110.172	+.0555137		.0554852	130.687	-.059	8481.

$\bar{\lambda}$ = 130.746 = ± .011

APPENDIX B

TABLE VII

WAVE LENGTHS OF CALIBRATION LINES

Element	Line	Wave Length in Seigbahn X Units	Reference
Tantalum	$K\alpha_1$	215.050 ± .010	a
Tungsten	$K\alpha_2$	213.382 ± .010	a
	$K\alpha_1$	208.571 ± .010	a
Tungsten - Gamma rays from W^{182}	68 Kev	182.638 ± .018	b
	100 Kev	123.599 ± .014	b

REFERENCES

a) E. Inglestam, Nova Acta Regiae, Soc. Sci. Upsalienis 4, No. 5, (1936)

b) Murray, Beehm, Marmier, and DuMond, Phys. Rev. 97, 1007 (1955)

APPENDIX C

BIBLIOGRAPHY

1. Bohr, A., Danske Mat. Fys. Medd. 26, No. 14 (1952)

2. Bohr, A. and B. R. Mottleson, Danske Mat. Fys. Medd. 27, No. 16 (1953)

3. Bragg, W. L., Proc. Cambridge Phil. Soc. 17, 43 (1912)

4. Cauchois, Y., Comptes Rendus 195, 1479 (1932)

5. Cauchois, Y., "Extension de la Spectrographie des Rayons X", Ann. Phys. 1, 215 (1934)

6. Cohen, E. R., J. W. M. DuMond, T. W. Layton, and J. S. Rollett, "Analysis of Variance of the 1952 Data on the Atomic Constants and a new Adjustment, 1955", Rev. Mod. Phys. 27, 363 (1955)

7. Chupp, E. L., A. F. Clark, J. W. M. DuMond, F. J. Gordon, and Hans Mark, "Precision Determination of the Low-Lying Energy Levels of W^{182}, W^{183}, W^{184}, and W^{186}", Phys. Rev. 107, 745 (1957)

8. Chupp, E. L., J. W. M. DuMond, F. J. Gordon, R. C. Jopson, and Hans Mark, "Precision Determination of Some Energy Levels in Fe^{57}, Zn^{67}, and Tc^{99}", Phys. Rev. 109, 2036 (1958)

9. Chupp, E. L., J. W. M. DuMond, F. J. Gordon, R. C. Jopson, and Hans Mark, "Precision Determination of Nuclear Energy Levels in Heavy Elements", Phys. Rev. 112, 518 (1958)

10. Davisson, C. M., and R. D. Evans, "Gamma Ray Absorption Coefficients", Rev. Mod. Phys. 24, 79 (1952)

11. DuMond, J. W. M., "High Resolving Power, Curved-Crystal Focusing Spectrometer for Short Wave-Length X-Rays and Gamma-Rays", Rev. Sci. Instr. 18, 626 (1947)

12. DuMond, J. W. M., "Crystal Diffraction Spectroscopy of Nuclear Gamma Rays", in "Beta and Gamma Ray Spectroscopy", Kai Siegbahn, ed., Interscience Publishers, New York, 1955

13. DuMond, J. W. M., "Spectroscopy of Nuclear Gamma Rays by Direct Crystal Diffraction Methods", in "Ergebnisse der Exakten Naturwissenschaften", Springer-Verlag, Berlin, 1955

14. DuMond, J. W. M. and E. R. Cohen, "Least Squares Adjustment of the Atomic Constants", Rev. Mod. Phys. 25, 691 (1953)

15. DuMond, J. W. M. and H. A. Kirkpatrick, "The Multiple Crystal X-Ray Spectrograph", Rev. Sci. Instr. 1, 88 (1930)

16. DuMond, J. W. M., D. A. Lind, and E. R. Cohen, "Precision Method of Generating Circular Cylindrical Surfaces of Large Radius of Curvature for Use in the Curved-Crystal Spectrometer", Rev. Sci. Instr. 18, 617 (1947)

17. Friedrich, Knipping, and Laue, "Bayer Akad. Wiss.", 1912; Le Radium, 10, 47 (1913)

18. Goldschmidt-Clermont, Annual Reviews of Nuclear Science, Vol. 3, Annual Review, Inc., Palo Alto, Calif., 1953

19. Johann, H. H., Z. Physik 69, 185 (1931)

20. Johansson, T., Z. Physik 82, 507 (1933)

21. Lind, D. A., W. J. West, and J. W. M. DuMond, "X-Ray and Gamma-Ray Reflection Properties from 500 X Units to Nine X Units of Unstressed and of Bent Quartz Plates for Use in the Two-Meter Curved-Crystal Focusing Gamma-Ray Spectrometer", Phys. Rev. 77, 475 (1950)

22. Richtmyer, F. K., E. H. Kennard, and T. Lauritsen, "Introduction to Modern Physics", 5th ed., McGraw-Hill, New York, 1955

23. Strominger, D., J. M. Hollander, and G. T. Seaborg, "Table of Isotopes", Rev. Mod. Phys. 30, 585 (1958)

24. Thompson, T. J. and T. Cantwell, "MITR: The MIT Research Reactor", Nucleonics 15, 38 (1957)

25. Watson, B. R., W. J. West, D. A. Lind, and J. W. M. DuMond, "Precision Study of the Tungsten K Spectrum Using the 2-Meter Focusing Curved Crystal Spectrometer", Phys. Rev. 75, 505 (1949)

26. Worthing, A. G. and J. Geffner, "Treatment of Experimental Data", John Wiley & Sons, New York, 1943

thesW225
Measurement of some rare earth gamma ray
3 2768 001 92930 0
DUDLEY KNOX LIBRARY